NOVA
NOVA SCHOOL OF SCIENCE & TECHNOLOGY

DEPARTAMENTO CIÊNCIAS DOS MATERIAIS

RAQUEL AZEVEDO MARTINS

Licenciada em Engenharia de Micro e Nanotecnologias

SOLUTION-BASED METAL OXIDE SEMICONDUCTOR MEMRISTOR

MESTRADO EM ENGENHARIA DE MICRO E NANOTECNOLOGIAS

Universidade NOVA de Lisboa

setembro, 2021

NOVA SCHOOL OF SCIENCE & TECHNOLOGY

DEPARTAMENTO DE CIÊNCIA DOS MATERIAIS

SOLUTION-BASED METAL OXIDE SEMICONDUCTOR MEMRISTOR

Raquel Azevedo Martins
Licenciada em Engenharia de Micro e Nanotecnologias

Orientador: Dr. Asal Kiazadeh, Researcher, CENIMAT-i3N, NOVA University Lisbon

Coorientador: Dr. Emanuel Abreu Antunes Carlos, Postdoctoral researcher, CENIMAT-i3N, NOVA University Lisbon

Júri:

Presidente: Professor Rodrigo Ferrão de Paiva Martins, Full Professor, DCM, NOVA University Lisbon

Arguente: Professor Rita Maria Mourão Salazar Branquinho, Invited Assistant Professor, DCM, NOVA University Lisbon

Vogal: Dr. Asal Kiazadeh, Researcher, Cenimat- i3N, NOVA University Lisbon

MESTRADO EM ENGENHARIA DE MICRO E NANOTECNOLOGIAS

Universidade NOVA de Lisboa
setembro, 2021

Solution-based Metal Oxide Semiconductor Memristor

Copyright © ⟨RAQUEL AZEVEDO MARTINS⟩, Faculdade de Ciências e Tecnologia, Universidade NOVA de Lisboa.
A Faculdade de Ciências e Tecnologia e a Universidade NOVA de Lisboa têm o direito, perpétuo e sem limites geográficos, de arquivar e publicar esta dissertação através de exemplares impressos reproduzidos em papel ou de forma digital, ou por qualquer outro meio conhecido ou que venha a ser inventado, e de a divulgar através de repositórios científicos e de admitir a sua cópia e distribuição com objetivos educacionais ou de investigação, não comerciais, desde que seja dado crédito ao autor e editor.

Acknowledgements

Seis anos que voaram e dou por mim sentada a culminar um curso numa dissertação de 30 páginas. Apesar de ser um trabalho individual, não posso deixar de agradecer às várias pessoas que contribuíram para o mesmo. Além disso, aproveito esta página para um momento de reflexão e nostalgia destes últimos anos.

Primeiramente, quero agradecer à minha instituição, NOVA School of Science and Technology da Universidade Nova de Lisboa e ao Departamento das Ciências dos Materiais. Agradecer também ao Professor Rodrigo Martins e à Professora Elvira Fortunato pela criação do curso de Engenharia de Micro e Nanotecnologias, assim como pela disponibilização do CENIMAT|i3N e CEMOP, locais de investigação com excelentes condições, que permitiu a realização desta dissertação.

Quero agradecer ao meu grupo de trabalho, a todos os que fazem parte do projeto NeurOxide e em especial, ao Jonas Deuermeier pela ajuda na caracterização dos dispositivos e à Maria Pereira pela disponibilidade em ajudar tanto na deposição dos elétrodos como no Keithley. Tenho de agradecer em particular, à minha orientadora Asal Kiazadeh, por estar sempre disponível para me ajudar e esclarecer ao longo destes meses. Ao meu orientador Emanuel Carlos, muito obrigado, pela disponibilidade, ajuda, preocupação e apoio, definitivamente este trabalho não teria corrido da mesma forma sem a sua presença. Foi sem dúvida uma escolha muito acertada e um privilégio trabalhar com os dois.

Aos meus colegas de faculdade que estiveram presentes nos mais diversos momentos, ao longo destes anos, obrigada. À malta do 2º esquerdo: Esteves, Madeira, Zé e Carvalho, obrigada por me receberem sempre em vossa casa de porta aberta. Ao Dmytro, Gui, Alentejano, Nia, Margarida, Edu, Leonor, Tânia e Tomás, obrigada por partilharem comigo esta viagem. Ao meu tropa de Massamá Diogo, obrigada. Foi preciso atravessar a ponte para criar uma amizade que me faz sentir sempre em casa. À Mariana Tomé e Mariana Moniz, companheiras que permanecem, só vos tenho a agradecer, vocês também andam comigo 'assim'. Obrigada por tudo.

A todas as minhas amigas de escola, obrigada por me acompanharem desde há muito. São amizades que me deixam muito orgulhosa e feliz, é um privilégio crescer ao vosso lado. Sim, estou a falar de vocês: Joana Palmeiro, Joana Reis, Rita, Abissa, Adriana, Ana, Laura e Mafalda.

Por fim, não posso deixar de agradecer à minha família, principalmente aos meus pais. Sou muito grata e sortuda por ser filha do Zé e da Almerinda. Ao meu primo Filipe, obrigada por seres uma inspiração e orgulho, este trabalho é dedicado a ti.

Resumo

Memristores baseados em processos de solução têm demonstrado um grande potencial para cumprir requisitos da Internet das Coisas (*IoT*), como dispositivos de elevada densidade e ultrabaixo consumo de energia aliado a métodos de fabrico simples e de baixo custo. Neste trabalho, filmes finos de óxido de índio-gálio-zinco (IGZO) são produzidos através do processo de síntese por combustão. Para melhorar o desempenho dos filmes de IGZO em memristores, são estudados diferentes parâmetros: a variação da proporção molar, o número de camadas depositadas e a temperatura de recozimento. Os memristores com maior número de camadas recozidas à temperatura mais elevada apresentam baixa tensão de operação, boa resistência, ótimo rendimento e retenção de até 10^5 s à temperatura ambiente. A melhor condição alcançada foi um memristor IGZO (1:3:1) com 7 camadas depositadas recozidas a 300 ºC. Estes dispositivos podem ser programados num em modo de operação multinível até 8 estados resistivos diferentes. Além disso, os mesmos dispositivos apresentam características promissoras para aplicações de computação neuromórfica, uma vez que conseguem emular a plasticidade de uma junção sináptica, ao replicar a potenciação e depressão de uma sinapse. Os resultados alcançados são bastante promissores e mesmo em alguns casos superam o atual estado da arte.

Keywords: IGZO, memristor baseado em processos de solução, síntese por combustão, sinapse artificial, Internet das coisas.

Abstract

Solution-based memristors have shown a great potential to fulfill several requirements of the Internet of Things (IoT) such as, high density and ultra-low power devices by using low-cost and simple fabrication methods. In this work, solution-processed indium-gallium-zinc oxide (IGZO) thin films are produced using a combustion synthesis process. To improve their performance in memristor devices different parameters are studied: the variation of molar proportion, number of deposited layers and annealing temperature. Memristors with higher number of layers and annealing temperatures show low operating voltage, good endurance, great yield, and retention up to 10^5 s in air environment conditions. The best condition reached was IGZO (1:3:1) memristor with 7 deposited layers annealed at 300 ºC. These devices can be programmed in a multi-level cell operation mode, up to 8 different resistive states. Furthermore, the same devices show promising features for neuromorphic computing applications since they can emulate the plasticity of a synaptic junction by replicating potentiation and depression. The results achieved are quite promising and even in some cases surpass the current state of the art.

Keywords: IGZO, solution-based memristor, solution combustion synthesis, metal oxides, artificial synapse, Internet of Things

Contents

List of Figures..........xv

List of Tables..........xvii

Symbols..........xix

Abbreviations..........xxi

Motivation and Objectives..........xxiii

1 Introduction 1

1.1 Amorphous Indium Gallium Zinc Oxide.......... 1

1.2 Solution-based Electronics 2

1.3 Solution Synthesis of Oxides.......... 2

1.4 Resistive Random-Access Memory (RRAM) Devices 3

1.5 Neuromorphic applications of Memristors 5

2 Materials and Methods 7

2.1 IGZO Precursor Solutions Preparation and Characterization.......... 7

2.2 IGZO Thin Films Deposition and Device Fabrication 7

2.3 IGZO Thin Films and Device Characterization.......... 8

3 Results and Discussion 9

3.1 IGZO Precursor Solution Characterization 9

3.1.1 Fourier Transform – Infrared Spectroscopy (FT-IR).......... 9

3.1.2 Differential Scanning Calorimetry and Thermogravimetry (DSC-TG).......... 9

3.2 IGZO Thin Film Characterization 10

3.2.1 Fourier Transform – Infrared Spectroscopy (FT-IR).......... 10

3.2.2 Optical Characterization 11

3.2.3 Scanning Electron Microscopy (SEM-FIB) 13

3.2.4 X-Ray Photoelectron Spectroscopy (XPS) 13

3.3 IGZO Memristors Electrical Characterization.......... 14

3.3.1 Direct Current (DC) sweep measurements 14

3.3.2 Pulse measurements.......... 19

3.3.3 Temperature Analysis.......... 21

4 Conclusions and Future Perspectives 24

5 References 26

Annexes.......... I

Annex A – IGZO Redox Reactions.......... I

Annex B – Calculation of E_{opt} of IGZO Thin Films.......... III

Annex C – XPS depth profile spectra' V
Annex D – Pristine Maps VI

List of Figures

Figure 1.1- Schematic that compares the energetics between two methods: sol-gel conventional process and solution combustion synthesis. 3
Figure 1.2 - Representation of electroforming. This step is essential because it promotes the formation of the CF and increases the Vo drift. In the beginning, the device is non polarized with only V_o near the Ti/Au contact. After electroforming, the V_o form the CF, and consequently polarizes the device. 4
Figure 1.3 - Schematic representation of the bipolar resistive switching in VCM-type devices. The SET occurs when a positive bias is applied, forming the CF, which changes the device state from LRS to HRS. The RESET happens when it is applied a negative voltage, breaking the CF, coming to its initial state (HRS). 5
Figure 2.1 - Schematic representation of the fabricated RRAM devices. 8
Figure 3.1 - FT-IR spectra of IGZO solutions with different molar ratios: 1:2:1 (black) and 1:3:1 (red)........ 9
Figure 3.2 - TG-DSC analysis of IGZO 1:2:1 and IGZO 1:3:1 precursor solution with 2-ME as solvent and urea as fuel........ 10
Figure 3.3 - FT-IR spectra's of IGZO thin films on Si substrates after annealing. (a) IGZO 1:2:1 thin film with 1, 3 and 5 layers, at 300 ºC; IGZO 1:3:1 thin film with 1, 3, 5 and 7 layers, at: (b) 200 ºC and (c) 300 ºC... 11
Figure 3.4 - Spectroscopy measurements of the IGZO thin films thickness (nm), for different annealing temperatures and molar ratios, on Si substrates: IGZO 1:3:1 annealed at 200 ºC (light green), IGZO 1:3:1 at 300 ºC (dark green) and IGZO 1:2:1 annealed at 30 ºC (orange)........ 11
Figure 3.5 - Transmittance spectra's of IGZO thin films on glass substrates.(a) IGZO 1:2:1 with several layers (1,3 and 5) annealed at 200 ºC; IGZO 1:3:1 with 1,3,5, and 7 layers annealed at (b) 200 ºC and (c) 300 ºC. 12
Figure 3.6 – SEM-FIB cross-section of a 5-layer IGZO device annealed at 300 ºC deposited onto a Si substrate. 13
Figure 3.7 - XPS surface spectra of samples with 5 IGZO (1:3:1) layers annealed at (a) 200 ºC and (b) 300 ºC. In both samples O 1s is deconvoluted into three main peaks. 14
Figure 3.8- Typical pristine state of IGZO memristors with different molar ration , number of layer deposited and annealing temperature: (a) IGZO 1:2:1 annealed at 300 ºC, (b) IGZO 1:3:1 annealed at 200 ºC and, (c) IGZO 1:3:1 annealed at 300 ºC. 15
Figure 3.9 - Yield of working devices in each condition, per sample (36 devices). 16
Figure 3.10 - I-V characteristics of electroforming step in IGZO 1:3:1 devices with 5 and 7 layers annealed at: (a) 200 ºC and (b) 300 ºC. 16
Figure 3.11 - I-V characteristics obtained from endurance tests during 100 cycles, in each condition: (a) 5 layers and (b) 7 layers at 300 ºC; (c) 5 layers and (d) 7 layers at 200 ºC. 17
Figure 3.12 – (a) Set and reset average voltage and (b) conductance fluctuation of on and off states of the I-V curves presented in Figure 3.12. 18
Figure 3.13 - Retention time of IGZO (1:3:1) memristor for 10^5 s with a read voltage at 0.1 V in air conditions: (a) 5 layers annealed at 200 ºC and (b) 7 layers annealed at 300 ºC. 18
Figure 3.14 - (a) MLC retention characteristics read at 0.1 V during 10^3 s for five different reset voltages and three set CC amplitudes; (b) corresponding reset and set I-V curves of each retention state........ 19
Figure 3.15 - Conductance response, under a 0.1 V read voltage, of a 7 layered device: (a) 100 consecutive pulses with positive voltage (potentiation) followed by 100 consecutive pulses with negative bias (depression); (b) 100 consecutive pulses with -0.8 V and 10 µs with different pulse intervals. 20
Figure 3.16 - (a) Schematic illustration of a biological synapse and a memristor; (b) Pulse scheme of potentiation; (c) Change of current during of 10 pulses with different pulse intervals; (d) Mean change of ΔI of (c). 21

Figure 3.17 - Temperature versus resistance dependency of LRS and HRS. LRS decreases its resistance as the temperature increase; HRS does not change its resistance with an increase of temperature. 22
Figure B.1 - Tauc-bandgap plots to calculate E_{opt} of each condition studied. III
Figure C.1 - XPS depth profile spectra after each etching of Ga $2p_{3/2}$, Zn $2p_{3/2}$, In $5d_{3/2}$ and Pt 4f of a 5 layered device annealed at 200 ºC. V
Figure C.2 – XPS depth profile spectra after each etching of Ga $2p_{3/2}$, Zn $2p_{3/2}$, In $5d_{3/2}$ and Pt 4f of a 5 layered device annealed at 300 ºC. V
Figure D.1 - Representation of a produced sample with Kapton tape. VI
Figure D.2 - Pristine maps of samples: IGZO molar proportion of 1:2:1 and annealed at 300 ºC, with 3 (left) and 5 layers (right). VI
Figure D.3 - Pristine maps of IGZO 1:3:1 samples with 3 layers annealed at 200 ºC (left) and 300 ºC (right). VI
Figure D.4 - Pristine maps of IGZO 1:3:1 samples with 5 layers annealed at 200 ºC (left) and 300 ºC (right). VII
Figure D.5 - Pristine maps of IGZO 1:3:1 samples with 7 layers annealed at 200 ºC (left) and 300 ºC (right). VIII

List of Tables

Table 1.1 - State of the art of solution-based IGZO memristors (S-RRAM). 1
Table 3.1 – Characteristic absorbance peaks and associated vibrational modes of the corresponding chemical bonds for analyzed FT-IR spectra of IGZO precursor solutions [71]. 9
Table 3.2 - Optical bandgap of the IGZO thin films produced in different conditions calculated by linear fit of Tauc-plots. 12
Table A.1 - Reduction and oxidation reactions. I
Table A.2 - Overall reaction given by the combination of reduction and oxidation reaction. I
Table A.3 - Valence of all reagents. I
Table A.4 - Number of moles (n) to ensure the stoichiometry of the redox reaction. II
Table A.5 - Overall reactions with the correct stoichiometry. II
Table B.1 - R^2 of each linear fit in Tauc plots.. IV

Symbols

α	Absorption coefficient
A	Optical absorption
d	Thickness
E_{opt}	Optical bandgap
φ	Fuel/oxidizer ratio
Φ_t	Thermal activation
h	Planck constant
h	Hours
I	Current
I_o	Initial current
v	Photon frequency
k	Boltzmann constant
M	Molar concentration
min	Minutes
°C	Degrees Celsius
n	Number of moles
rpm	Rotations per minute
R	Reflectance
$R_{ON/OFF}$	On-off resistance ratio
R^2	Coefficient of determination
rms	Surface roughness
s	Second
S	Siemens
T	Temperature
V	Voltage
V_O	Oxygen Vacancies
V_{SET}	Set voltage
V_{RESET}	Reset voltage
χ^2	Error function
Ω	Ohm

Abbreviations

2-ME	2-Methoxyethanol
AFM	Atomic Force Microscopy
AI	Artificial Intelligence
ALD	Atomic Layer Deposition
ANNs	Artificial Neural Networks
ATR	Attenuated Total Reflectance
CC	Current Compliance
CEMOP	Center of Excellence in Microelectronics and Optoelectronic Processes
CENIMAT	Centro de Investigação de Materiais
CF	Conductive Filaments
CMOS	Complementary Metal-oxide-semiconductors
CVD	Chemical Vapor Deposition
DC	Direct Current
DIW	Deionized Water
DSC	Differential Scanning Calorimetry
ECM	Electrochemical Metallization Mechanism
FIB	Focused Ion Beam
FT-IR	Fourier Transform-Infrared Spectroscopy
HRS	High Resistance State
IGZO	Indium-gallium-zinc Oxide
IoT	Internet of Things
IPA	Isopropyl Alcohol
I-V	Current-Voltage
LRS	Low Resistance State
MIM	Metal-Insulator-Metal
MLC	Multi-Level Cell
MRAM	Magnetoresistive Random-Access Memory
NIR	Near Infrared
NVM	Non-Volatile Memory
OV	Oxidation Valence
PCRAM	Phase Change Random-Access Memory
PLD	Pulsed Laser Deposition

PPF	Pair-Pulse Facilitation
RAM	Random-Access Memory
RRAM	Resistive Random-Access Memory
RS	Resistive Switching
RV	Reduction Valence
SCS	Solution Combustion Synthesis
SEM	Scanning Electron Microscopy
S-RRAM	Solution-Based Resistive Random-Access Memory
STDP	Spike-Time-Dependent Plasticity
TAOS	Transparent Amorphous Oxide Semiconductor
TFT	Thin Film Transistor
TG	Thermogravimetry
TCM	Thermochemical Mechanism
UV	Ultraviolet
VCM	Valence Change Mechanism
XPS	X-Ray Photoelectron Spectroscopy

Motivation and Objectives

Nowadays, technology is everywhere, and it will be even more present in the future due to the Internet of Things (IoT). This concept defines the “intelligence” of devices to connect and communicate with each other. Devices connection to IoT require high velocity, more storage memory and lower energy consumption, which is hard and expensive to obtain with the current electronic components. In silicon-based technology, it is not possible to integrate logic and non-volatile memory (NVM) components due to their incompatibility in integration flow [1].

Therefore, emergent memories have appeared as an alternative since they are compatible with complementary metal-oxide-semiconductors (CMOS) and can be produced at large scale reducing the associated costs. One strong candidate is the resistive random-access memory (RRAM) or also called memristor, since it fulfills the characteristics needed for IoT devices. A very attractive advantage is that RRAM allows low-cost integration by combining CMOS-friendly materials within a simple two-terminal device structure. Besides, RRAM devices can be fabricated by solution-based processes with similar reliability that vacuum techniques have but with lower costs and simpler fabrication methods. Solution-based memories have the desirable electronic characteristics, being an option to future electronic applications. However, these memories are emerging and have a lot of unknown factors making it imperative to continue the studies in this field.

The main objective of this work is to study, produce and optimize solution-based indium-gallium-zinc oxide (IGZO) memristors (S-RRAM), using metal nitrates as precursors with the benefits of solution combustion synthesis (SCS) to produce the active layer of the RRAM devices. To accomplish that, several tasks will be employed:

- Production and characterization of IGZO thin films with different molar proportions;
- Production and characterization of memristors devices using different thicknesses and temperature.

1 Introduction

Electronic devices are mostly based on silicon technology. However, with the development of transparent, flexible and paper electronics, there is the need to find other materials to fulfill these new technologies [2], [3]. Transparent amorphous oxides semiconductors (TAOSs) materials are an alternative, since they have excellent optical transparency and electrical properties [4]. TAOSs usually have their valence band occupied with 2p O anti-bonding states and the conduction band has unoccupied ns metal bonding [5]. These electron configuration benefits the electron transport, giving these materials a high carrier mobility (> 10 $cm^2V^{-1}s^{-1}$) [5], [6]. Besides the great optical and electrical properties, TAOSs can be processed at low temperatures which turns the processes less expensive and more environment friendly [2]. Nowadays, a TAOS widely used in electronic is IGZO.

1.1 Amorphous Indium Gallium Zinc Oxide

IGZO has attracted a lot of attention since is a potential material for flexible transparent electronics. The main application is in thin film transistors (TFTs) for flat-panel applications [7], [8]. Indeed, IGZO is used as an active layer in TFTs concerning its high transparency, high mobility and stability [7], [9]. Furthermore, in the right molar proportion IGZO also exhibits great resistive switching (RS) properties [10], which makes this material an option for RRAM devices.

It is well known that electrical characteristics of the IGZO TFTs rely on the indium and gallium composition [11]. An increase in indium concentration will enhance the mobility, whereas an increment in gallium concentration will decrease the generation of oxygen vacancies (V_o) [12], [13]. The presence of Zn is relevant to develop an amorphous structure, promotes flexibility, which is needed when applied in flexible substrates [2]. With a stoichiometry of 3:1:1 (In/Ga/Zn) commonly used in TFTs [14], it is possible to identify RS characteristics. However, this condition has problems in terms of stability and switching mechanism [8], being important the optimization of the right stoichiometry to achieve better IGZO RRAM devices.

Focusing on gallium concentration, as mentioned, plays a role on generation of V_o, which is one of the responsible for carrier transport. Increasing the content of gallium changes completely the characteristics in the defect density and insulating properties [8], proving that is possible to control the local resistivity [15]. Hereupon, by controlling the concentration of gallium, it is a way to obtain devices made of IGZO for different applications: more gallium will promote the RS mechanism, which is the intended for the memory devices, while in TFTs the goal is to have less gallium and more indium to benefit from a high mobility [7].

Solution-based memristors are still an emergent technology, particularly, IGZO S-RRAM are very recent in the science community, as demonstrated by Table 1.1.

Table 1.1 - State of the art of solution-based IGZO memristors (S-RRAM).

Year	**T_{max} (ºC)**	**Bottom/Top electrode**	**Switching Behavior**	**$R_{ON/OFF}$**	**Retention (s)**	**Endurance (cycles)**	**MLC***	**Neuro-morphic Applications**
2012 [8]	370	Al/Al	Bipolar	2.7	n.d.	10^2	No	No
2014 [7]	300	Pt/Ti	Bipolar	3×10^1	10^4	9×10^1	No	No
2014 [9]	130	Pt/Pt	Bipolar and Unipolar	>10	10^4	10^2	No	No

2017 [16]	350	Ti/Ti	Bipolar	>10	10^4	10^2	No	No
2018 [17]	150	ITO/Pt	Bipolar	Aprox 10^3	10^4	10^4	No	No
2020 [18]	250	Ni/Pt	Unipolar	Aprox 10^2	10^4	2.5×10^2	No	No
2021 [19]	350	Al/ITO	n.d.	n.d.	n.d.	n.d.	Yes	Yes
2021 [20]	Microwave Annealing	Pt/Ti	Bipolar	10^1	10^4	10^3	Yes	Yes
This Work	200	Ti/Pt	Bipolar	10^2	10^5	10^2	No	No
	300	Ti/Au	Bipolar	10^2	10^5	10^2	Yes	Yes

*Multi-Level Cell

1.2 Solution-based Electronics

In order to guarantee the best features in inorganic materials for memory applications, the techniques mostly used are based on vacuum processes. The most common are: chemical layer deposition (CVD)[21], plasma oxidation [22], thermal oxidation [23], pulsed layer deposition (PLD)[24], magnetron sputtering [25]–[27] and atomic layer deposition (ALD)[28]. These techniques produce high-quality devices, with a good performance and reliability. On the other hand, these methods have several disadvantages, such as high cost, time consumption and require a controlled environment [29], [30].

Solution-based processes can surpass these challenges. Not only the fabrication is simpler, lower cost and with low temperature, but also the performance of the device is comparable with the ones made in vacuum environments [31]–[35]. With this approach is possible to achieve large area manufacturing without expensive methodologies [36] by using coating (dip-coating, spin-coating, spray-coating) and printing techniques (inkjet printing, screen printing) [16], [37], [38].

These techniques allow the use of other materials besides the conventional silicon (Si), for the same electronic applications. Solution-based metal oxide TFTs are one example and the most studied product using these techniques [39]. But, after the discovery of the memristor, researchers started to publish more about oxide thin films RS devices, like RRAM [36]. These memories can be produced using these low cost methods, which is a promising path for future flexible electronics. Currently, the most used technique is spin coating, however, in the future, the goal is to produce these devices using printing methods which are compatible with large scale manufacturing [36].

1.3 Solution Synthesis of Oxides

Although, S-RRAM uses simpler fabrication methods, it is crucial to consider some solution synthesis parameters since the ambient conditions and the fabrication method influence the overall device performance [36]. Normally, these devices are manufactured by sol-gel method [18], [40], more precisely, by the metal-salt sol-gel chemistry [41], [42]. This method consists of forming precursor solutions followed by several chemical reactions until it forms a gel [43]. Typically, that solution is deposited by a printing or coating technique and then submitted to annealing at high temperatures, to form a metal oxide thin film [44]. However, since it is important to reduce the temperature during the fabrication process, solution combustion synthesis (SCS) has

been proving to be more suitable. This method is simple, practical and efficient in a lot of applications, one of them TFTs [14], [32], [45], [46]. It is also a scalable, fast, low cost and reproducible way to create nanostructures and thin films [47].

SCS is described as a self-sustained redox reaction initiated by a source of energy between a fuel and an oxidant in metal cations' presence. Usually the oxidant are metal nitrates and the fuel has carbon and hydrogen in its composition to facilitate the liberation of heat by forming H_2O and CO_2 during the combustion process [47]. The main advantage when adding a fuel in a sol-gel method, is that it is possible to form metal oxide lattices with a low ignition temperature (Figure 1.1). When a fuel is present, applying just a moderate temperature is enough to trigger the combustion reaction, leading to a strong exothermic redox reaction with energy to convert precursors into oxides [47]. Therefore, SCS is a viable way to form metal oxides from precursors solutions at low temperatures, resulting in thin films with high homogeneity and purity [36].

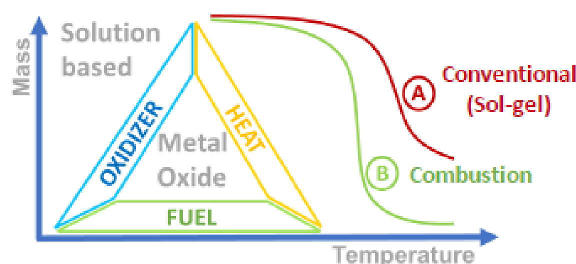

Figure 1.1- Schematic that compares the energetics between two methods: sol-gel conventional process and solution combustion synthesis [47].

1.4 Resistive Random-Access Memory (RRAM) Devices

The RS phenomenum has been present for several decades, being for the first time detected in oxide materials [48]. During the last century, researchers also reported the first RS cell [49] and the RS behavior in magnetoresistive films [50]. However, only in 2008, it started to gain relevance by being connected to neural networks and logic circuits, beginning the concept of memristor [51]. RRAM is one of the main candidates to join other CMOS technology, since it is a simple metal-insulator-metal (MIM) structure, where usually the insulator is a transition metal oxide [1], [36]. Indeed, RRAM devices have stood out due to their potential, since it has simple structure, high density and operation speeds and low power consumption. These properties frame as an option in memory solution for the next generation of non-volatile memories (NVM) [18].

NVM are characterized by their ability to store information for a long period of time (over 10 years) and retain information without a power supplier, unlike volatile memories. Beyond that, this technology has the ability to perform with low consumption, high endurance, high operation speed, small size, and high-density capacity [52]. Nowadays, NAND Flash memories are the most used NVM [53], [54], but emergent NVM devices like RRAM or memristor [55], [56], magnetoresistive RAM (MRAM) [57], [58] and phase change RAM (PCRAM) [59] are a promising potential technology for NVM devices. Moreover, RRAM are even better than NAND Flash memories, insofar they have the same features, although with better switching speed, endurance, and future scalability. RRAM and PCRAM can also storage intermediate resistance states, as they operate based on the rearrangement of atomic configurations, which gives them a larger window for storage [36].

Focusing only on RRAM, this type of memory is characterized by an electrical reversible RS mechanism, between a low resistance state (LRS) and a high resistance state (HRS) [1]. To switch from different states, mostly RRAM cells need to execute an electroforming step to activate the RS [60]. These states are achieved by redox reactions that create and break conductive filaments (CF) when temperature and/or electrical voltage is applied. These redox-based resistive mechanisms typically can be classified as: valence

change mechanism (VCM), electrochemical metallization mechanism (ECM) and thermochemical mechanism (TCM).

ECM is a cation-based mechanism that usually uses an electrochemical active metal (Cu, Ag) for the active layer and exhibits bipolar switching due to the formation and dissolution of the CF at different voltage polarities[61], [62]. When applied an electrical voltage, the electroforming process ionizes the metal atoms and causes the electromigration of metal cations through the resistive switching layer, which causes the variation of internal resistance. Normally, it is chosen electrolytic materials with high ion conductivity and low electron conductivity to produce ECM devices [1]. TCM is based in both cation and anion motion and occurs when the thermochemical redox process dominates over the electrochemical process, so it is a thermal process. TCM switching happens when there is an increase of the temperature, causing variations of stoichiometry and redox reactions which leads to an alteration of the local conductivity. Because of this, TCM has a unipolar switching behavior, that is, formation and dissolution of CF occurs in the same polarity, depending only on voltage magnitude [61], [63].

VCM is based in an anion/oxygen-ion mechanism, where redox reactions are connected to the solid-state transport of ions at nanometer length scales. VCM occurs when an external electrical field is applied causing a redox reaction expressed by a valence change of the cation sublattice and consequently a change in electronic conductivity [60], [64]. As RS behavior is dependent of the charged ionic defects, VCM is inherently bipolar, that is the polarity of the voltage determines if it occurs oxidation or reduction. Thus, SET and RESET operation occur at the opposite voltage polarities [60]. Generally, VCM cells structure consists of one high work function inert metal (for instance Pt or Au) to assure a Schottky barrier and the other metal is based on a low work function metal (commonly Ta, Hf, Ni, Al and Ti) being the ohmic contact [61], [65]. Regarding to the active layer, the participation of a transport of anions is essential for the RS, whence transition metal oxides are suitable for this purpose. In this material, oxygen ion defects (V_o) are much more mobile than transition metal cations, so when there is a enrichment or a depletion of V_o, this will affect the valence state of the transition metal cations, leading to an alteration in the electronic conductivity [60].

As mentioned before, to activate the RS in the devices it is required to perform an electroforming step. For this, a high voltage is applied to the device, forming a conductive filament (CF) in the oxide that connects the two electrodes, allowing the current passage and turn-on the device, as despite in Figure 1.2. Since most of the RS processes in transition metal oxides devices based on VCM depends on oxygen exchange reactions, the electrodes/metal oxide interface play a key role in their operation [1].

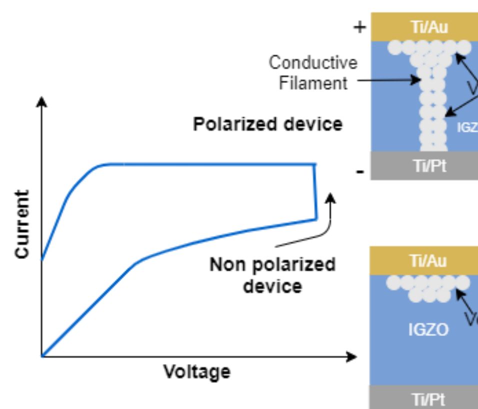

Figure 1.2 - Representation of electroforming. This step is essential because it promotes the formation of the CF and increases the Vo drift. In the beginning, the device is non polarized with only V_o near the Ti/Au contact. After electroforming, the V_o form the CF, and consequently polarizes the device.

It is considered that most of the V_o are created in the oxide/ohmic contact interface [65]. With this electronic connection, the temperature in the device rises considerably due to the joule heating, allowing the creation and movement of the V_o. However, the created electric field in the oxide must be formed with a current compliance (CC) or else it leads to a hard breakdown of the device. To achieve the high resistance state (HRS), it is applied voltage with the opposite polarity, causing the redistribution of the V_o and consequently break of the CF previously formed, as observed in Figure 1.3. Taking into account that these processes are reversible, applying the original voltage polarity can reconnect the CFs, altering from HRS to LRS and vice versa [1], [65].

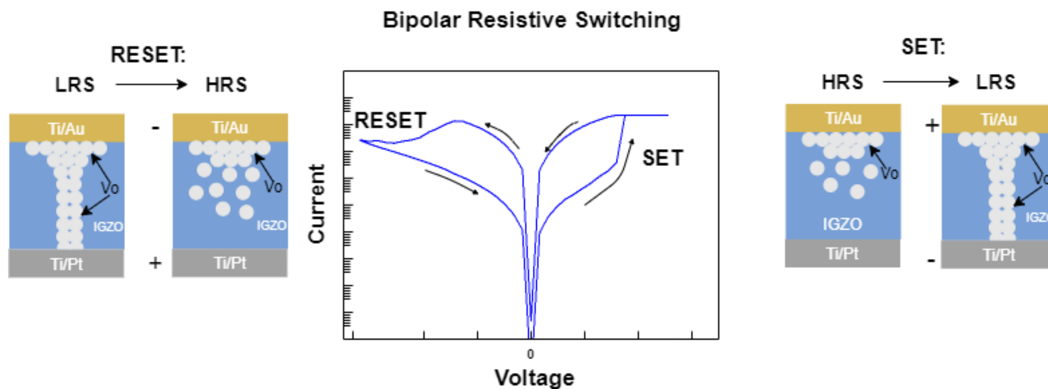

Figure 1.3 - Schematic representation of the bipolar resistive switching in VCM-type devices. The SET occurs when a positive bias is applied, forming the CF, which changes the device state from LRS to HRS. The RESET happens when it is applied a negative voltage, breaking the CF, coming to its initial state (HRS).

1.5 Neuromorphic applications of Memristors

Traditional Von Neumann's architecture for computing systems is getting to its limitations in terms of miniaturization and data process. One of the reasons is that this model is not able to process data simultaneously, which compromises its velocity and efficiency [66]. Neuromorphic computing urged to overcome these issues. It is a brain-inspired approach, that is suitable to solve complex and parallel processing with low power consumption [67].

The human brain can perform perception, learning and memory functions by connecting the neurons through synapses. The modulation of the strength between the neurons is due to the plasticity characteristic present in the synapses [68]. There are billions of neurons and trillions of synapses in the brain, that perform learning and memory processes at the same time with an extraordinary energy-efficiency. As neuromorphic computing is a system that emulates the human brain, there has to be a device that reproduces the synaptic functions.

One of the biggest interests on memristors is for neuromorphic applications as a synaptic device [66]. Memristor has a simple structure and an electrical behavior that is capable of emulating a synapse. The resistance of the memristor works as synaptic weight and it is controlled by the voltage or current induced [69]. Also, the possibility of scalability, the low power consumption, and data retention characteristics of the memristor makes these devices ideal to replicate the synaptic behavior in an artificial neural networks (ANNs) circuit.

Neuromorphic systems using ANNs are capable of high density processing and storage. With memristors in a circuit emulating synapses it is possible to create perception and motion systems for artificial intelligence (AI) [70].

2 Materials and Methods

This section summarizes the procedures and techniques used during this work, since the production of IGZO solutions to the fabrication and characterization of IGZO memristors.

IGZO memristors were studied by varying the molar ratio of metallic cations, the annealing temperature and the number of active layers, to determine the best condition to obtain a memristor with a good electrical performance.

2.1 IGZO Precursor Solutions Preparation and Characterization

The metallic oxide precursor solutions were prepared by dissolving individually indium (III) nitrate hydrate ($In(NO_3)_3 \cdot xH_2O$, Sigma-Aldrich, 99.9%), gallium (III) nitrate hydrate ($Ga(NO_3)_3 \cdot xH_2O$, Sigma-Aldrich, 99.9%) and zinc nitrate hexahydrate ($Zn(NO_3)_2 \cdot 6H_2O$, Sigma-Aldrich, 98%) in 2-methoxyethanol (2-ME, $C_3H_8O_2$, Fisher Chemical, 99%), to produce solutions with a concentration of 0.2 M. For the combustion reaction, urea ($CO(NH_2)_2$, Sigma-Aldrich, 99.0-100.5%) was added as fuel to each precursor solution, with molar ratios between urea and each metallic oxide of (5/2):1, (5/2):1, (5/3):1 for indium, gallium and zinc nitrate, respectively, to assure the redox stoichiometry of the reaction (Annex A). All precursor solutions were magnetically stirred at 430 rpm for 1h at room temperature in air environment.

The IGZO semiconductor precursor solutions were prepared by mixing the precursor solutions made, indium nitrate, gallium nitrate and zinc nitrate, to obtain In:Ga:Zn molar ratios of 1:2:1 and 1:3:1, all with 0.2 M concentration. These solutions were magnetically stirred at 430 rpm for at least 36 h at room temperature in air environment to form a homogenous and transparent solution. IGZO precursor solutions were filtered through 0.2 µm hydrophilic filters.

Thermal and chemical characterization of precursor solutions were performed by Differential Scanning Calorimetry (DSC) and Thermogravimetry (TG) and Fourier Transform-Infrared Spectroscopy (FT-IR). DSC-TG analysis were prepared by evaporating 10 mL IGZO precursor solution for 5 hours. The measurements were executed under air atmosphere up to 550°C with a 10°C/min heating rate in an aluminum crucible using a simultaneous thermal analyzer, Netzsch (TGA-DSC-STA 449 F3 Jupiter). FT-IR spectroscopy characterization of IGZO solutions was performed using Atenuated Total Reflectance (ATR) sampling accessory (Smart iTR) equipped with a single bounce diamond crystal on a Thermo Nicolet 6700 Spectrometer, between 4500 cm^{-1} and 525 cm^{-1}.

2.2 IGZO Thin Films Deposition and Device Fabrication

Preceding the deposition, all substrates (soda-lime glass, area of $2.5\times2.5cm^2$) were cleaned in an ultrasonic bath at 50 °C in acetone for 10 min, then in Isopropyl Alcohol (IPA) for the same time. Afterwards, the substrates were cleaned with deionized water (DIW) and then, they were dried under N_2 and put on a hotplate at 110 °C for 10 min.

Following the cleaning process, a 30-nm-thick Ti and a 30-nm-thick Pt layers were deposited by e-beam evaporation onto the glass substrates as bottom electrode. To prepare the substrate for the films deposition, they were submitted to an Ultraviolet (UV)/Ozone surface activation step for lamp distance of 7 cm with no temperature for 15 min, using a PSD-UV Novascan system.

Before the deposition by spin coating, it was used Kapton tape to cover one border of the substrates, to access the bottom electrode when performing electrical characterization. Several IGZO thin films were deposited onto Pt/Ti substrates by sequentially spin coating. 1, 3, 5 and 7 layers of IGZO precursor solutions were spun for 35s at 2000 rpm with an acceleration of 1500 rpm/s (spinner Laurell Technologies), followed by an immediate hotplate annealing at 200 °C or 300 °C for 30 min after each layer, in ambient conditions (20

ºC with 60 % of humidity), to ensure the exothermic reaction. Between each layer deposition plus annealing, the substrates were always submitted to an UV treatment with no temperature for 10 min to improve the adhesion of subsequent layers. To complete the device, a 6-nm-thick Ti and 60-nm-thick Au were deposited by e-beam evaporation as top electrode, using a shadow mask. The Ti/Au contacts pattern are a 6×6 matrix, resulting 36 working devices in each sample. The contacts varied from 0.5 to 1 mm of diameter. All fabricated devices used the same architecture: Glass/Ti/Pt/IGZO/Ti/Au, represented in Figure 2.2.

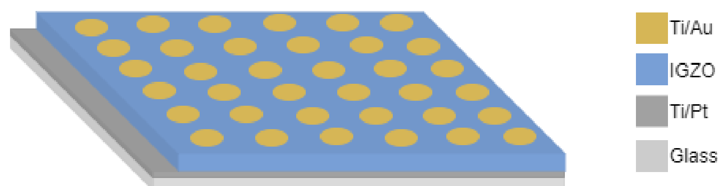

Figure 2.2. - Schematic representation of the fabricated RRAM devices.

2.3 IGZO Thin Films and Device Characterization

To study the effect of the number of active layers, IGZO precursor solutions were deposited in the same conditions onto soda-lime glass and onto silicon oxide (SiO_2) substrates.

Spectroscopic ellipsometry was used to measure the thin film thickness deposited on SiO_2 substrates, with an energy range from 1.5 to 5.5 eV and an incident angle of 45° using Yvon Uvisel system. The acquired data were modulated using the DELTAPSI software and the fitting procedure was done pursuing the minimization of error function (χ^2). FT-IR spectroscopy characterization of thin films deposited in SiO_2 substrates was performed the same way as used for IGZO precursor solutions. The optical properties were obtained by a Perkin Elmer lambda 950 UV/Visible/Near Infrared (NIR) spectrophotometer. The transmittance (T%) of the thin films deposited on glass substrates was obtained in a wavelength range from 250 to 2500 nm. Pictures for observation and analyses of the thin films deposited on glass were acquired using an Optical Microscope – Olympus BX51.

The devices were also studied by scanning electron microscopy (SEM) using a Zeiss Auriga Crossbeam electron microscope. A cross section on the produced devices was made by focused ion beam (FIB). X-Ray Photoelectron Spectroscopy (XPS) measurements were also performed on the devices by a Kratos Axis Supra spectrometer to study the composition. A monochromatic Al K α source was used with an aperture of 110 µm and the analyzer was set to pass energy of 80 eV. For depth profiling, an argon cluster of 500 atoms was used, with a kinetic energy of 10 keV, and scanned over 1.5 mm^2. The data were analyzed with CasaXPS software. Atomic force microscopy (AFM, Asylum MFP3D) was performed on substrates with Pt/Ti to investigate the impact of temperature used in the bottom electrode during annealing in the final devices.

Electrical characterization was performed by measurement of current-voltage characteristics of the devices using a semiconductor parameter analyzer (Keithley 4200 SCS) attached to a microprobe station (Janis ST-500) at room temperature. The voltage was applied to the top electrode maintaining the bottom electrode connected to ground. The speed of the measurements was at normal mode and the integration time was in autosetting. Measurements with controlled temperature (273 K to 373 K) were performed by a Cryogenic controller (Lakeshore 336) in air conditions.

3 Results and Discussion

This chapter presents and discusses the results concerning the characterization of solutions, thin films and also, the electrical characterization of the produced memristors.

3.1 IGZO Precursor Solution Characterization

3.1.1 Fourier Transform – Infrared Spectroscopy (FT-IR)

FT-IR, using ATR, was performed to analyze the elements through characteristic spectra of IGZO solutions using 2-ME as solvent and urea as fuel. Figure 3.1. illustrates the FT-IR spectra of IGZO precursor solutions for each molar ratio studied, with data in wavenumber range of 4000-525 cm^{-1}. Table 3.1 [71] identifies the peaks, that are mostly related with organic compounds present in 2-ME.

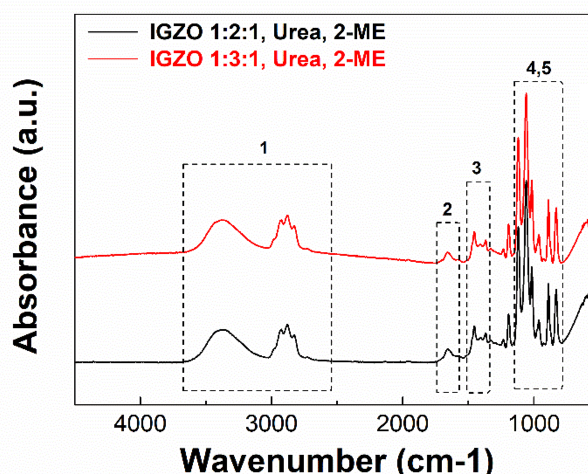

Figure 3.1. - FT-IR spectra of IGZO solutions with different molar ratios: 1:2:1 (black) and 1:3:1 (red).

Table 3.1 – Characteristic absorbance peaks and associated vibrational modes of the corresponding chemical bonds for analyzed FT-IR spectra of IGZO precursor solutions [71].

Number	Position (cm^{-1})	Mode type	Chemical Bond
1	3500	Stretching vibration	M-OH
2,4	1620, 1015	Bending vibration	M-OH
3	1388	Stretching vibration	NO_3^-
5	833	Bending vibration	NO_3^-

3.1.2 Differential Scanning Calorimetry and Thermogravimetry (DSC-TG)

To evaluate the decomposition behavior of the metal oxide precursors, a thermal analysis was performed. Figure 3.2. shows the DSC-TG results for IGZO solutions, with different molar ratios (1:2:1 and 1:3:1) for comparison.

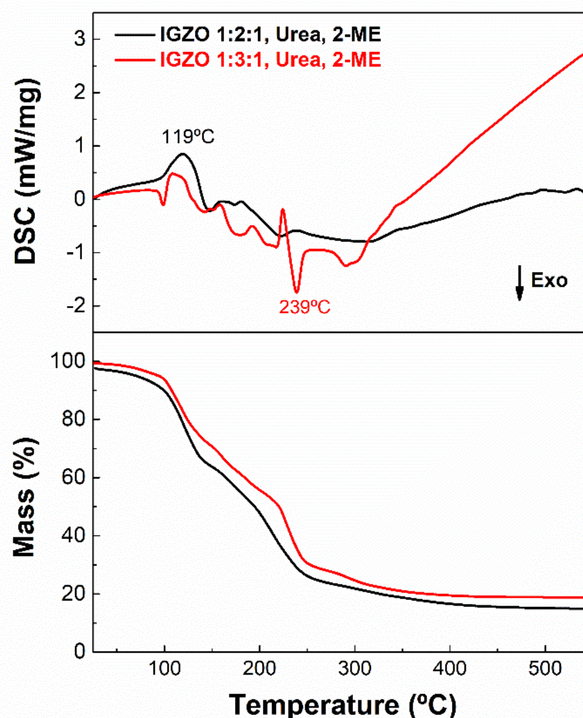

Figure 3.2 - TG-DSC analysis of IGZO 1:2:1 and IGZO 1:3:1 precursor solution with 2-ME as solvent and urea as fuel.

Regarding IGZO 1:2:1 solution, DSC graph shows a broad endothermic peak at 119 ºC accompanied by a substantial mass loss of 31 %. This reaction is related to the evaporation of residual solvents present in the solution [72]. IGZO 1:3:1 exhibits one main exothermic peaks at 239 ºC, accompanied with mass loss of 33 %. This peak corresponds to the redox reaction of the formation of oxides [72]. In both IGZO molar proportions, thermal analysis reveal that the minimum temperature required for full degradation is near 250 ºC. To reduce the temperature required for the complete degradation of residual organics, UV irradiation can be used during the annealing process.

However, the heating rate and the previous evaporation solvent step can strongly influence the DSC-TG analysis. During the previous solvent evaporation, the urea present in the solutions could initiate combustion reactions, unbalancing the stoichiometry.

3.2 IGZO Thin Film Characterization

3.2.1 Fourier Transform – Infrared Spectroscopy (FT-IR)

In order to analyze the chemical bonds present in IGZO after thin films fabrication, FT-IR was performed in the same conditions as mentioned before. Figure 3.3 shows the FT-IR spectra for all the conditions studied.

Comparing with FT-IR analysis of IGZO precursor solution, the peaks related to solvent and nitrate bonds are no longer present after the thin film production. Moreover, the peaks related to M-O bonds at 620 cm^{-1} are even more defined after the annealing process, confirming the formation of metal oxides.

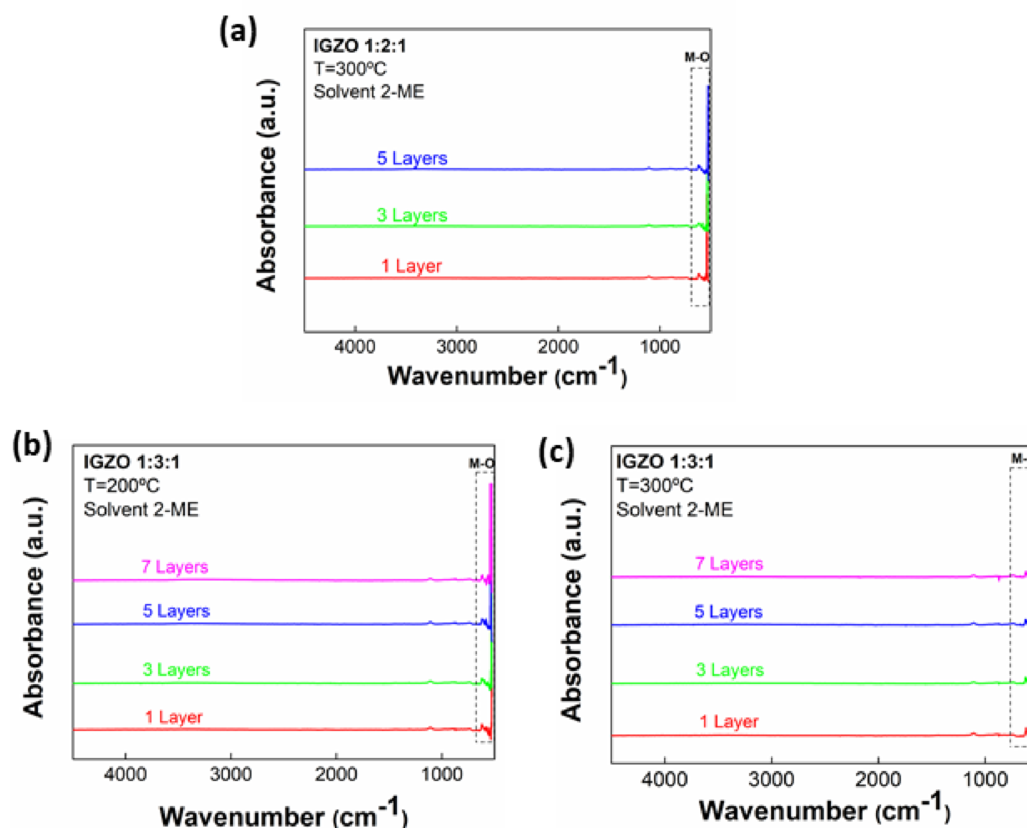

Figure 3.3 - FT-IR spectra's of IGZO thin films on Si substrates after annealing. (a) IGZO 1:2:1 thin film with 1, 3 and 5 layers, at 300 ºC; IGZO 1:3:1 thin film with 1, 3, 5 and 7 layers, at: (b) 200 ºC and (c) 300 ºC.

3.2.2 Optical Characterization

For optical characterization, spectroscopy ellipsometry was used to measure the thickness of all thin films. The thickness values for each molar ratio and temperature are presented in Figure 3.4. It is noteworthy that the model used during the measurements could influence the results, since the molar proportion specified did not include more quantity of gallium.

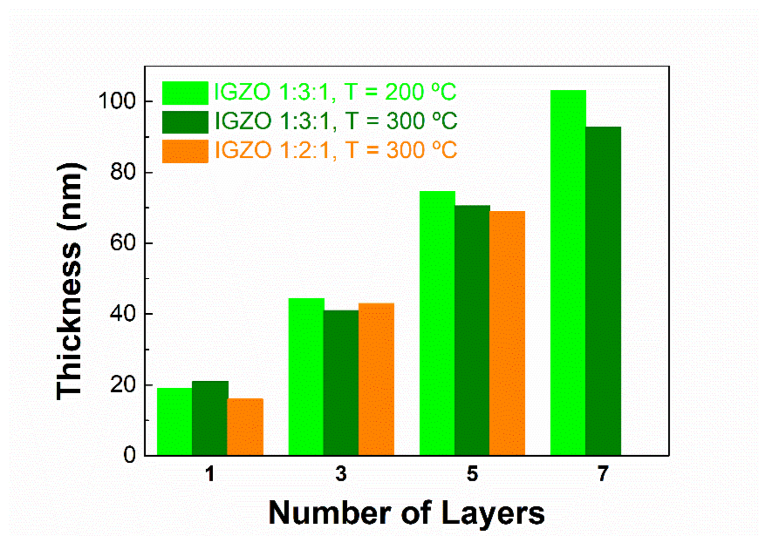

Figure 3.4 - Spectroscopy measurements of the IGZO thin films thickness (nm), for different annealing temperatures and molar ratios, on Si substrates: IGZO 1:3:1 annealed at 200 ºC (light green), IGZO 1:3:1 at 300 ºC (dark green) and IGZO 1:2:1 annealed at 300 ºC (orange).

Thickness values are similar for the same number of layers, in spite of the molar proportion and temperature. However, in the case of the IGZO (1:3:1) annealed at lower temperature films are thicker when compared with samples annealed at 300 ºC with the same number of layers due to lower thin films densification. Annealing temperature is crucial for film densification, higher temperatures form denser metal oxide thin films better for electrical performance [36].

UV-visible spectroscopy was performed to observe the transparency of the thin films. Transmittance spectra were obtained in a wavelength range of 200-2500 nm, for each IGZO thin film, as shown in Figure 3.5. The transmittance values are near 90 % in the visible range. However, the increase of layers depositions, and consequently the thickness, affect the transmittance values, lowering from 90 to 86 %. Also, it was observed that as the number of deposited layers increase the transmittance decreased which is correlated with the spectroscopy measurements.

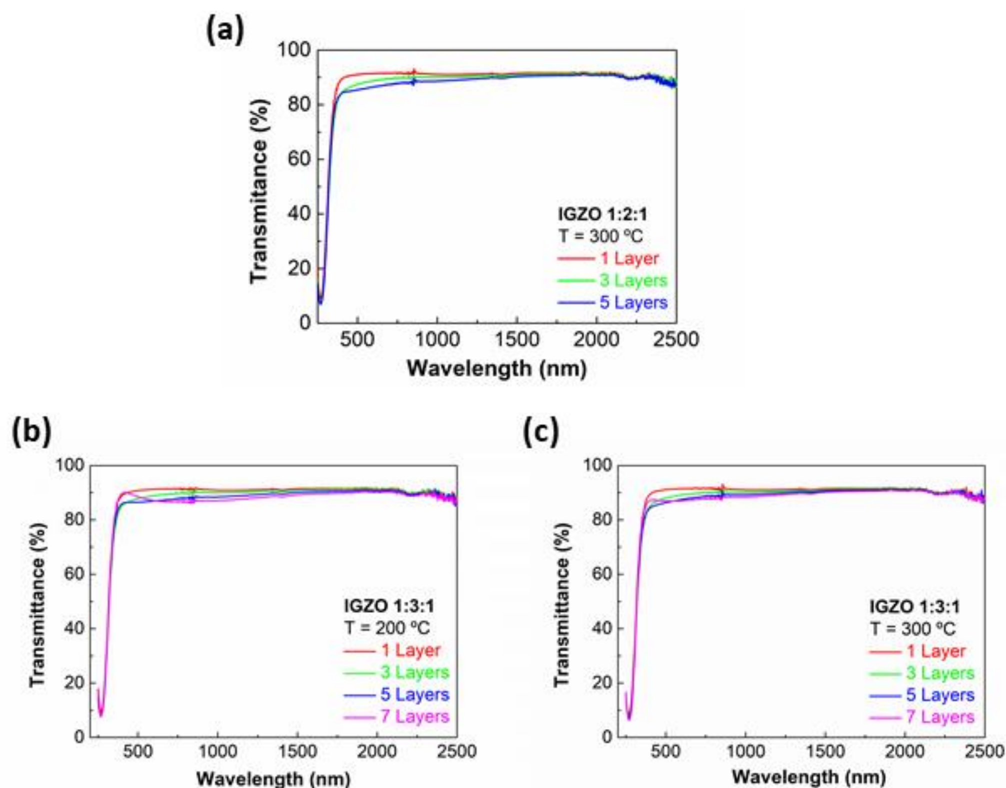

Figure 3.5 - Transmittance spectra's of IGZO thin films on glass substrates.(a) IGZO 1:2:1 with several layers (1,3 and 5) annealed at 200 ºC; IGZO 1:3:1 with 1,3,5, and 7 layers annealed at (b) 200 ºC and (c) 300 ºC.

The optical bandgap (E_{opt}) of each IGZO thin film was calculated through Tauc-bandgap plots, as depicted in Table 3.2. Tauc plots and calculation steps are detailed in Annex B.

Table 3.2 - Optical bandgap of the IGZO thin films produced in different conditions calculated by linear fit of Tauc-plots.

Number of Layers	Optical bandgap (eV)		
	200 ºC	300 ºC	
	1:3:1	1:3:1	1:2:1
1	3.29	3.28	3.31
3	3.25	3.23	3.28
5	3.28	3.24	3.35
7	3.30	3.29	———

In multicomponent oxides, the atomic composition of each cation affects the E_{opt} values, which usually is more closed to the E_{opt} of the dominant cation. In case of IGZO, the optical bandgap depends on the values of In_2O_3, Ga_2O_3 and ZnO, which theoretically are 3.5-3.7 eV, 4.16 eV and 3.2-3.4 eV, respectively [73] . Therefore, for IGZO 1:2:1 and 1:3:1 (with atomic ratio of 2:4:1 and 2:6:1, respectively), it is expected to obtain E_{opt} closer to the values obtained in literature for Ga_2O_3, since there is a dominance in Ga concentration. Nevertheless, the calculated values are in a range of 3.23 to 3.35 eV, regardless the composition, meaning that the produced films have the E_{opt} required for optical transparent electronics. Yet, these variations can be associated to the quantity of indium and zinc present [73].

3.2.3 Scanning Electron Microscopy (SEM-FIB)

SEM-FIB cross-section image of a solution-based IGZO (1:3:1) memristor is shown in Figure 3.6. This is an example of the structure obtained for a device with 5 IGZO layers annealed at 300 ºC on a Si substrate.

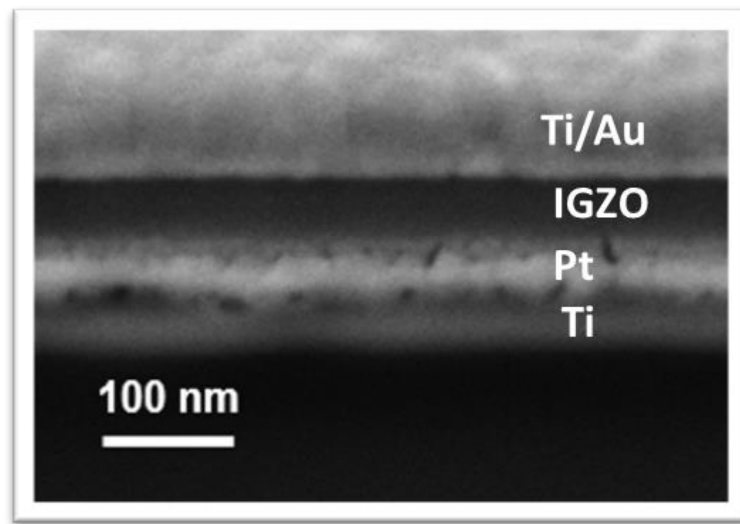

Figure 3.6 – SEM-FIB cross-section of a 5-layer IGZO device annealed at 300 ºC deposited onto a Si substrate.

The average thickness of the constituent layers of the memristor were measured using the ImageJ software. The thickness of the bottom and top electrode is approximately the values defined in e-beam evaporation (60 and 66 nm, respectively). In case of the active layer, here IGZO has an approximate thickness of 50 ± 0.2 nm, which is less than ellipsometry measurement (70.5 nm) performed in the same sample.

3.2.4 X-Ray Photoelectron Spectroscopy (XPS)

To evaluate the differences of the IGZO (1:3:1) thin films with 5 layers annealed with different temperatures was performed XPS measurements. Figure 3.7 depicts the film's surface in both samples, where O 1s is deconvoluted into three main peaks: 531.03, 532.21 and 533.48 eV at 200 ºC; and 531.46, 532.66 and 533.65 eV at 300 ºC. Each peak is related to components present on the surface. The first corresponds to M-O-M bonds, the middle peak is associated to M-OH or with undercoordinated oxygen and the last peak is due to water and organic species adsorbed on the surface [14]. The values obtained agree to the literature found [9].

Comparing the peaks intensity between samples, M-O-M bonds peak is more intense at 300 ºC, meaning that this condition has more oxygen-metal bonds present at the surface. At 200 ºC is less intense, there are less M-O-M bonds present and so other elements are present in the film, which indicates that the redox reaction may not be complete. The peak related to M-OH bonds is more evident at 200 ºC meaning that this sample has

more oxygen vacancies, and its more conductive. In comparison with the sample annealed at 300 ºC, the same peak is less intense, so the film is more insulating due to the presence of less M-OH bonds. The intensity of the last peak indicates that the presence of water and organic species is similar in both samples. Nevertheless, this existence of weakly bound oxygen species on the film's surface disappears after the etching.

Depth profile spectra' were obtained to study the structure along the samples. The etching time for both samples were 100 s and the results are presented in Annex C. By analysis of the profiles at both temperatures, there is a soft shift to lower binding energies of In $3d_{5/2}$, Ga $2p_{3/2}$ and Zn $2p_{3/2}$ elements as the etching reaches to the interface with Pt. With the approximation to the Pt electrode, there are more metallic states, that were not present before and this occurs at the same time the etching profile detects Pt 4f. An explanation to this is the uneven distribution of V_o in the active layer. The V_o are more concentrated near the top electrode and only when it forms the CF, the V_o are distributed along the active layer until the bottom contact. So, the IGZO near to the Pt is less oxidized and has more metallic states [1].

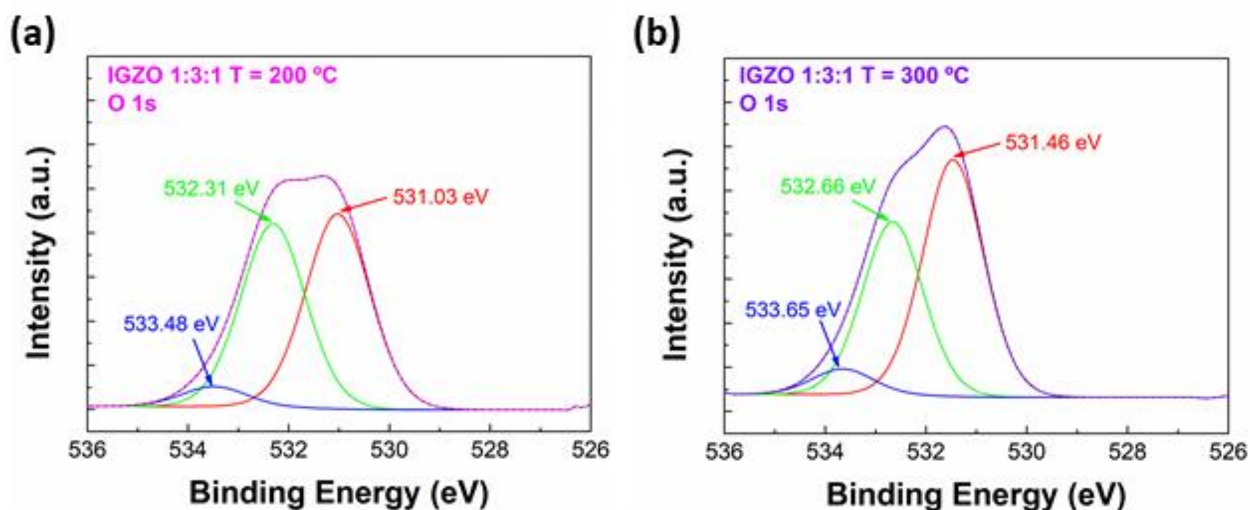

Figure 3.7 - XPS surface spectra of samples with 5 IGZO (1:3:1) layers annealed at (a) 200 ºC and (b) 300 ºC. In both samples O 1s is deconvoluted into three main peaks.

3.3 IGZO Memristors Electrical Characterization

3.3.1 Direct Current (DC) sweep measurements

The main purpose of this work was the optimization of the active layer of solution-based IGZO thin films and their applications in memristors. The electrical characterization is a fundamental part of this study, so it was performed the measurement of the current-voltage (I-V) curves of each device. By this analysis it is possible to understand their electrical behavior, properties, and future applications.

The first I-V characteristics obtained in each device are the pristine state to know if the device is electrical insulating or conducting [1]. For all devices, a voltage sweep was applied from -0.5 V to 0.5 V under a CC. The delimitation of a CC is crucial to prevent the hard breakdown of the devices. Figure 3.8 shows the typical pristine state in each studied condition. Here, it is evident the effect of the number of layers on the decrease of conductivity. The increment of the thickness corresponds also to an increase of oxygen vacancies (V_o), leading to more resistive devices. In both IGZO 1:3:1 annealing temperatures condition, 7 layers devices show very low current values. In a memristor, it is important to have an insulating behavior but with enough V_o to conduct the current and change its resistance state when voltage is applied.

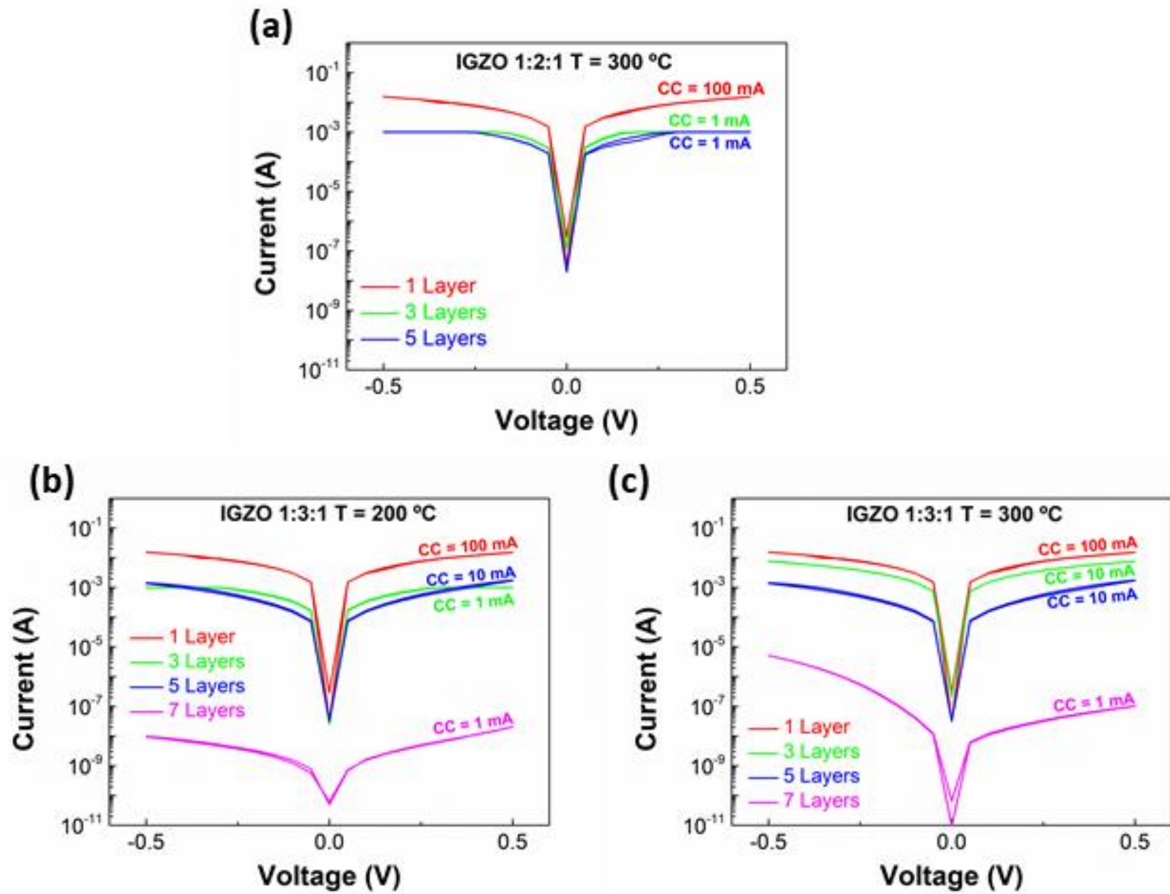

Figure 3.8 - Typical pristine state of IGZO memristors with different molar ration , number of layer deposited and annealing temperature: (a) IGZO 1:2:1 annealed at 300 ºC, (b) IGZO 1:3:1 annealed at 200 ºC and, (c) IGZO 1:3:1 annealed at 300 ºC.

The optimization of the memristors can be analyzed through the yield obtained in each sample. For that, it was performed the pristine state of every device of each sample, to reveal the number of working devices expected in each sample. Annex D contains the pristine maps made, standing out the working devices in green. It is noteworthy that in every studied condition, all pristine maps revealed that the side of the sample where it was applied Kapton tape had most of the working devices, unlike the opposite side of the sample, which had almost nonfunctional device. There is where it has more accumulation of IGZO precursor solution and consequently, a thicker active layer.

The yield calculations are presented in Figure 3.9. By comparing IGZO molar ratios, it is clear that IGZO 1:3:1 has more potential for memristor performance, with more yield at both temperatures. This is due to the increased Ga concentration, that suppresses the V_o formation, resulting in more resistive devices. Regarding temperature, IGZO 1:3:1 samples show better yield results at higher temperature, reaching a yield of 53 % in the sample with 7 layers. This can be explained by the temperature required to the complete formation of the metal oxides, as revealed in DSC-TG analysis, which is above 200 ºC. Samples annealed at 200 ºC have more organic residues than desirable in the active layer, which harms the electrical performance and the uniformity of the sample, resulting in lower yields. Also, there is a significant difference between 5- and 7-layer condition were the yield improved substantially, indicating that the annealing time and number of layers can promote the densification of the films and elimination of defects (e.g. fill of pores in the thin film) obtaining better electrical characteristics.

Therefore, the most appropriate molar proportion for a good memristor performance can be considered IGZO 1:3:1 [8], with the appropriate ratio of gallium. In terms of thin film deposition, an increase of layers has a positive impact on the yield, regardless of the annealing temperature used.

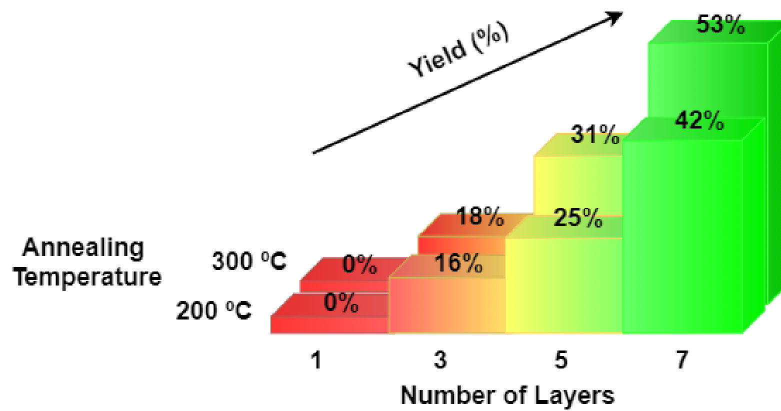

Figure 3.9 - Yield of working devices in each condition, per sample (36 devices).

Since pristine state and yield results revealed poor electrical performance at IGZO molar proportion of 1:2:1, the electrical tests and analysis were pursued with the IGZO memristors with a molar proportion of 1:3:1 with 5 and 7 layers, annealed at 200 and 300 ºC.

As mentioned previously in introduction, to activate the RS mechanism it is necessary an electroforming step, to form the CF. Figure 3.10. shows the electroforming curves for devices with different annealing conditions. Regarding memristors produced at 200 ºC, the voltage required to form CF was 3 V for a 5-layer device and 1 V for a 7 layered one. However, the CC used was different, so if the CC of the 7 layer device was also 10 mA, the electroforming response would require more voltage. In case of memristors annealed at 300 ºC, with 5 layers the device formed at 1.8 V whereas with 7 layers the device required 2.5 V to form. It was expected that the voltage applied to electroform the devices would be higher with the increase of layers (active layer is more resistive), which is the case of devices produced with higher temperature. The presence of residual organics in the active layer interfere with the CF formation and also with uniformity. So, devices produced at 200 ºC, shows all these issues in the electroforming step, and it arose the need of increasing the CC to obtain a response. Solution-based processes used do not guarantee uniformity within the sample, being more noticeable in samples with lower annealing temperatures as shown in pristine state maps and electroforming plots.

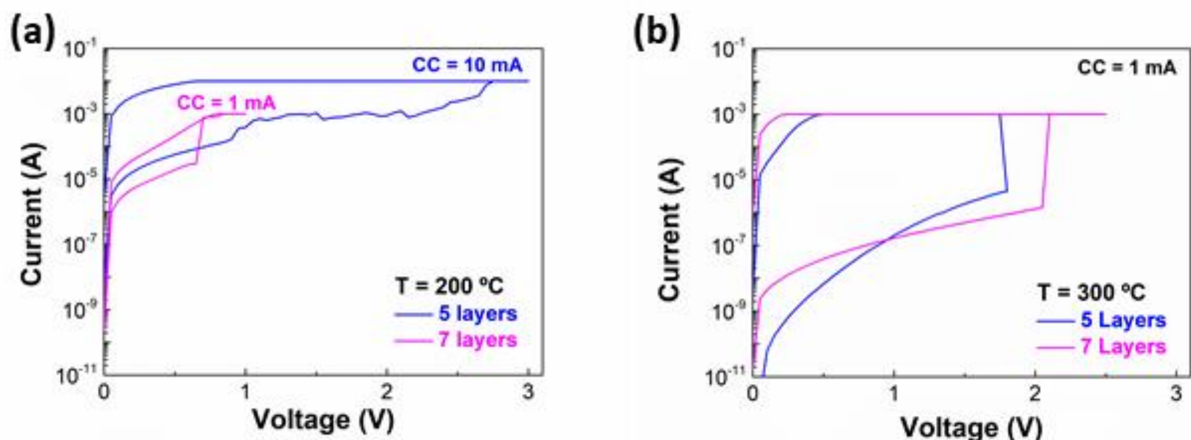

Figure 3.10 - I-V characteristics of electroforming step in IGZO 1:3:1 devices with 5 and 7 layers annealed at: (a) 200 ºC and (b) 300 ºC.

After electroforming step, the RS behavior was analyzed through endurance tests, as shown in Figure 3.11. The I-V curves were obtained with consecutive DC sweeps under a fixed voltage and CC. In every condition, memristors revealed bipolar RS behavior, with an abrupt set on the positive polarity and a gradual reset under negative bias. Except device with 5 layers annealed at 200 ºC, which has the same polarity response, but with an abrupt set and reset curves. Once the devices are programmed with a set and a reset voltage, cycling tests shows good endurance and stability of the memristors.

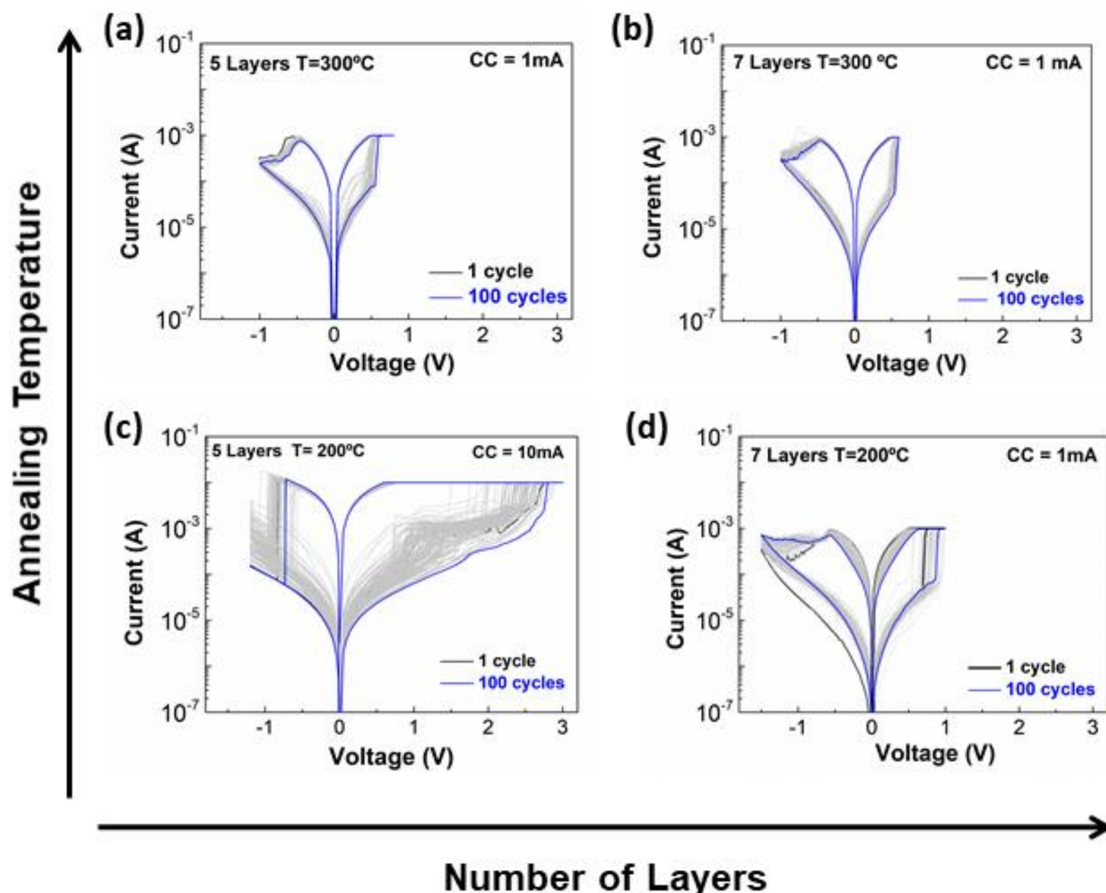

Figure 3.11 - I-V characteristics obtained from endurance tests during 100 cycles, in each condition: (a) 5 layers and (b) 7 layers at 300 ºC; (c) 5 layers and (d) 7 layers at 200 ºC.

Although, the increase of the number of layers and annealing temperature helps to reduce the devices variability , as depicted in Figure 3.12. The analysis of conductance fluctuation shows that both on and off states have larger variations in devices annealed at 200 ºC, whereas devices produced at 300 ºC have a similar and smaller fluctuations.

The results achieved are in accordance with the material characterization to form memristors with good performance being required high annealing temperatures [36]. As DSC-TG analysis revealed, 200 ºC do not guarantee high quality films to form the active layer of memristors, since the redox reaction may not be complete. Also, XPS results show that samples annealed at 300 ºC have higher quantity of M-O-M bonds and an insulating behavior, characteristics needed for a good memristor electrical performance. Nevertheless, by increasing the number of active layers can attenuate this problem, as demonstrated by pristine curves and yield.

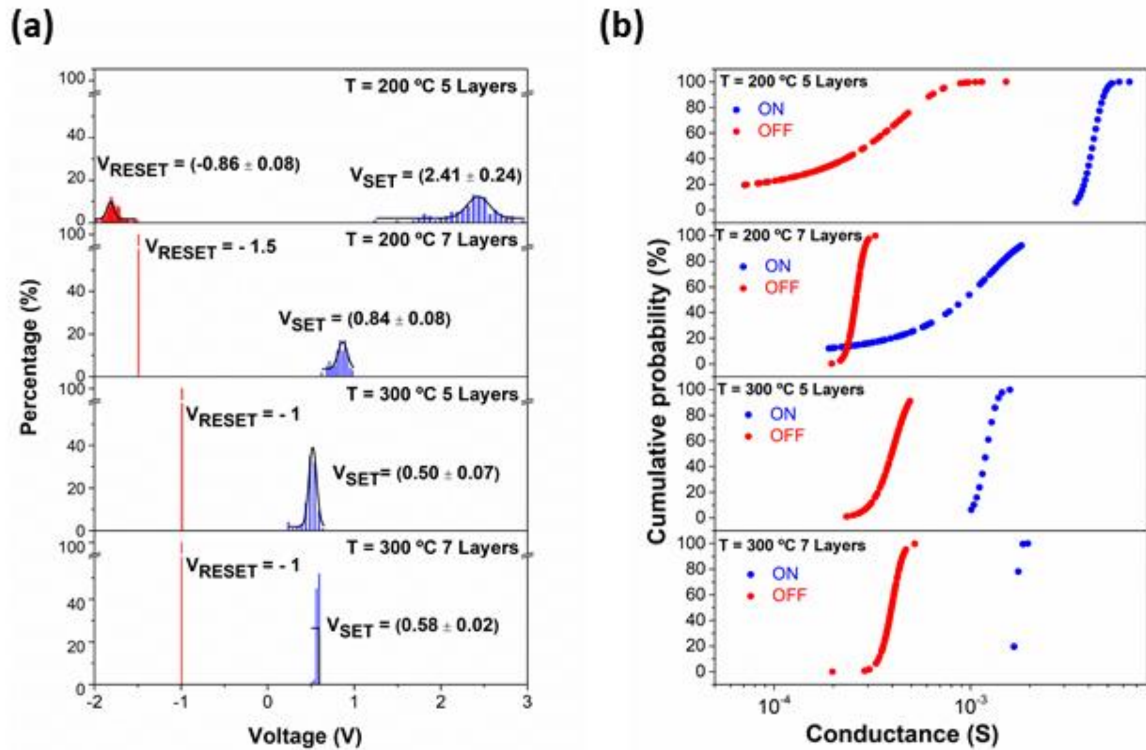

Figure 3.12 – (a) Set and reset average voltage and (b) conductance fluctuation of on and off states of the I-V curves presented in Figure 3.11.

In order to evaluate the devices volatility, retention tests were performed as presented in Figure 3.13. Both tests were performed under air conditions for 10^5 s with read voltage at 0.1 V. The results show good stability of LRS and HRS with no degradation over time, meaning that the produced devices are considered non-volatile memories. For both annealing temperatures, the $R_{ON/OFF}$ is 10^2 , however, devices annealed at 300 ºC are more resistive when compared with the ones produced at 200 ºC. Once again, it is perceptible that the electrical performance is dependent of the annealing temperature. The resistivity of the memristor is clearly affected by the annealing temperature used. When applied higher annealing temperatures there is an improvement in film densification and a decrease of current paths [36], leading to more resistive devices.

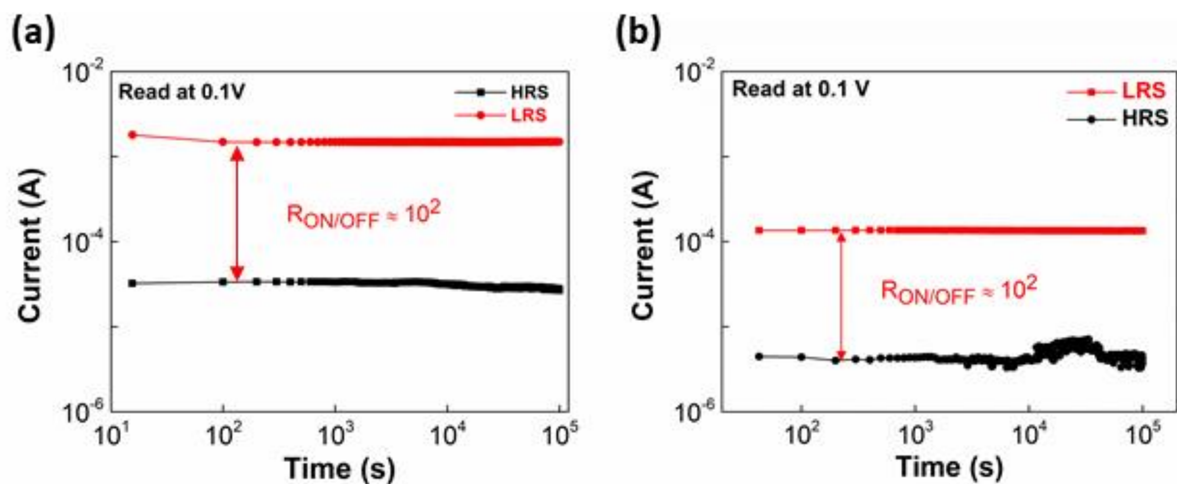

Figure 3.13 - Retention time of IGZO (1:3:1) memristor for 10^5 s with a read voltage at 0.1 V in air conditions: (a) 5 layers annealed at 200 ºC and (b) 7 layers annealed at 300 ºC.

Since the presented devices are considered non-volatile memories and have a $R_{ON/OFF}$ of 10^2 , I-V curves and retention tests were performed to see multi-level cell (MLC) behavior. That is, the possibility to program more than two resistive states in a memristor to achieve high densification [33]. Figure 3.14 represents the

states programmed on the device and respective set and reset I-V curves in Figure 3.14 (b). Every resistance state obtained had a retention of 10^3 s with a read voltage at 0.1 V.

To obtain MLC behavior the device was programmed in two different modes. First, it was programmed with a reset stop voltage, starting from the onset of the negative resistance. Then, the last three states were programmed through CC control, with a fixed voltage. This resulted in a memristor with a capacity to storage 3 bits per cell, which corresponds to eight different resistance states.

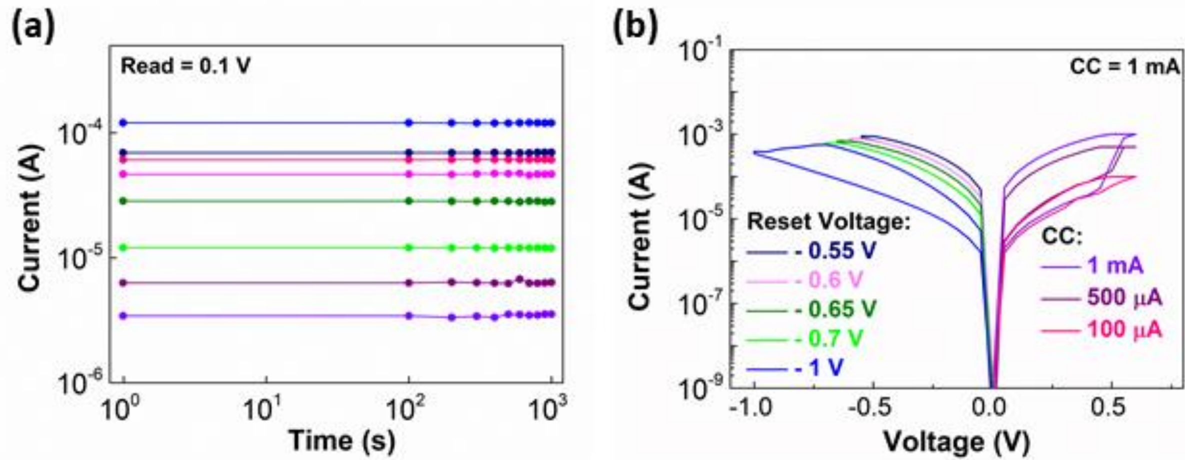

Figure 3.14 – Memristor with 7 layers annealed at 300 ºC: (a) MLC retention characteristics read at 0.1 V during 10^3 s for five different reset voltages and three set CC amplitudes; (b) corresponding reset and set I-V curves of each retention state.

3.3.2 Pulse measurements

The capacity of MLC storage arose the possibility to use these memristors for neuromorphic ends, since it is a feature demanded for this application [74]. The pulse measurements presented in this work are a preliminary study of these devices and were performed only on devices with 7 layers annealed at 300 ºC.

To simulate the behavior of a synapse in a memristor, a continuous electrical pulse must be applied. With that, the device emulates the plasticity of a synapse, potentiation or depression, depending on the polarity of the applied pulse. Figure 3.15 (a) presents the conductance response to 100 positive consecutive pulses (potentiation) followed by 100 negative pulses (depression), under a 0.1 V read voltage. Respecting potentiation, both conditions of pulse amplitude and width achieve the same conductance values, however the conductance change is abrupt. A way to improve that is to reduce the voltage amplitude used to replicate potentiation. On the other hand, in depression the pulse with -1 V of voltage and 10 µs of width cannot recover to its initial state. Here, both conditions have a more gradual decrease in conductance.

Another test that was performed is showed in Figure 3.15 (b), where the pulse amplitude and width was kept the same (-0.8 V and 10 µs) and the pulse intervals (20 ns and 1 µs) was changed to observe gradualness in conductance response. Pulses with 10 µs apart have a more gradual response when compared with the response of pulses 20 ns apart. A gradual response allows the device to achieve many resistive states, which is important for synaptic applications [74]. Pulse interval is critical for gradual response in these devices once the increase of the pulse interval makes the response much more gradual with the same pulse condition. Although the current range is not as large as the on/off ratio obtained in DC sweep, once it is an analog current change. Besides, the synaptic response is improved when a proper pulse condition is applied.

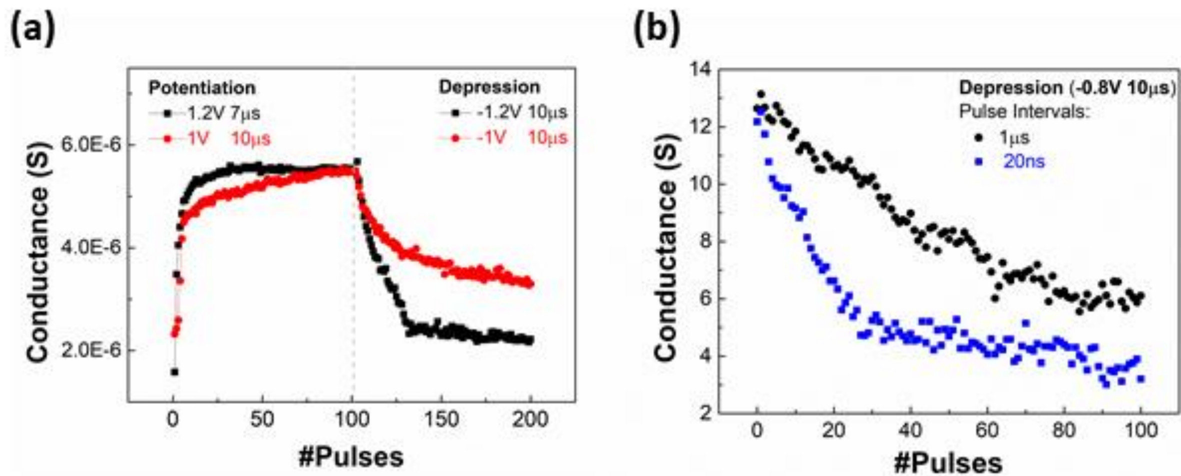

Figure 3.15 - Conductance response, under a 0.1 V read voltage, of a 7 layered device: (a) 100 consecutive pulses with positive voltage (potentiation) followed by 100 consecutive pulses with negative bias (depression); (b) 100 consecutive pulses with -0.8 V and 10 µs with different pulse intervals.

A neuromorphic device intends to perform in a same way as a biological synapse with the similar characteristics. The connection between neurons is modulated by their plasticity changing its synaptic weight [66]. In a memristor, there is an analogous behavior, as illustrated in Figure 3.16 (a). The device forms a conductive paths connecting the bottom and top electrodes, that can also be altered by applying different voltage amplitudes.

One feature present in synapses is spike-time-dependent plasticity (STDP). This means that the synaptic weight can be modulated by timing differences between pre- and pos-synaptic spikes [67]. In an artificial synapse, using different pulse intervals affects the conductance change at the end, observing STDP. Figure 3.16 (b) shows a schematic of potentiation with pulse amplitude of 0.9 V and width of 20 µs, followed by a pulse read with 0.1 V and 20 ms. Four different tests were performed with a combined pulse with different intervals (5 ms, 1 ms, 500 µs and 100 µs), as depicted in Figure 3.16 (c) and (d). In Figure 3.16 (c), the bars corresponds to the current increase in each pulse, and in Figure 3.16 (d) ΔI indicates the gain in current after the first pulse both from the same data. If the interval between pulses is smaller the current does not have enough time to come back to its initial state, and after consecutive pulses reaches higher current states. However, in this work the devices are not patterned, which does not guarantee if the device is in the same initial state in all tests performed. But, it is conclusive that smaller intervals between pulses helps the potentiation process, creating a pair-pulse facilitation (PPF) effect, important for learning functions [68].

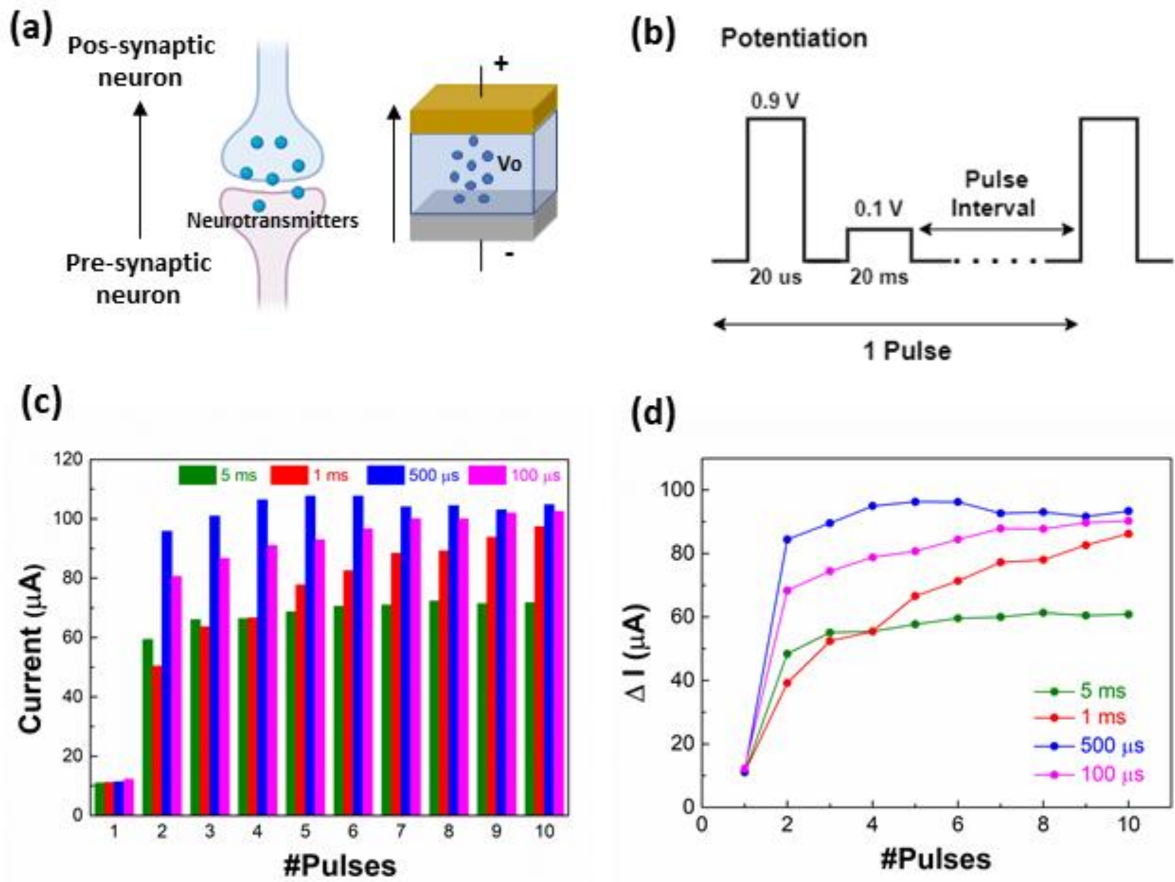

Figure 3.16 - (a) Schematic illustration of a biological synapse and a memristor; (b) Pulse scheme of potentiation; (c) Change of current during of 10 pulses with different pulse intervals; (d) Mean change of ΔI of (c).

3.3.3 Temperature Analysis

As final step of this work, temperature analysis was performed to study the conduction behavior of the produced memristors. For this test it was used the best device condition, the one with 7 layers annealed at 300 ºC. The measurements were performed under air ambient conditions, and the resistance values correspond to the device in LRS and HRS. The temperature range used was from 300 K to 420 K.

Figure 3.17 represents the temperature dependence of LRS and HRS. The thermal analysis reveals that LRS resistance decreases with the increase of temperature, with an approximate direct proportion of LRS ∝ T, which describes a typical semiconductor behavior [75]. The current (I) dependency with temperature (T) is described by Equation 1

$$I = I_o \exp(-\phi_t \, kT) \quad (1)$$

where k is the Boltzmann constant and ϕ_t is the thermal activation energy [75]. At HRS (off-state), temperature dependency is very weak, the resistance has no visible change as the temperature increases.

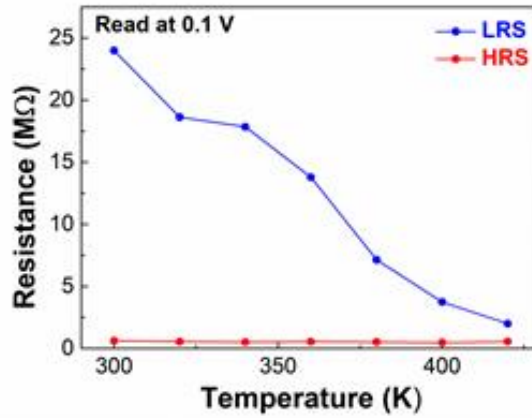

Figure 3.17 - Temperature versus resistance dependency of LRS and HRS. LRS decreases its resistance as the temperature increase; HRS does not change its resistance with an increase of temperature.

Based on the results presented above, the bipolar mechanism of these memristors are due to the variation of the oxygen-deficiency in IGZO, confirming that V_o are responsible for the conduction in these memristors The change of states between HRS and LRS happens when a voltage is applied resulting in the movement of oxygen ions to form or corrupt conductive paths in the active layer [7].

4 Conclusions and Future Perspectives

The focus of this work was the production and characterization of solution-based IGZO memristors; and also, the optimization of the active layer by producing IGZO thin films with different molar proportions, thicknesses and annealing temperatures.

First, IGZO solutions with molar proportions of 1:2:1 and 1:3:1 were produced by SCS, using urea as fuel and 2-ME as solvent. Then, memristors were fabricated on a glass substrate using e-beam evaporation to deposit the electrodes and spin-coating to deposit several layers of IGZO that were annealed at 200 or 300 ºC.

Solution characterization was done by FT-IR and DSC-TG. FT-IR spectra showed the expected peaks that are mostly related to the solvent. DSC-TG study revealed that 200 ºC was not enough to complete the redox reaction, essential to form metal oxides and high densify thin films. For both IGZO molar proportions studied (1:2:1 and 1:3:1), the minimum temperature required to complete the redox reaction to form the metal oxides was near 300 ºC.

As for thin film characterization, FT-IR was performed and it was observed that the peaks related to the solvent were gone, due to the annealing step in the thin film fabrication. Regarding optical characterization, spectroscopy ellipsometry allowed to determine the thickness variation of devices with different processed conditions. IGZO 1:3:1 memristors are thicker at 200 ºC comparing with the ones annealed at 300 ºC with the same number of layers. Transparency and bandgap values were obtained by UV-visible spectroscopy and Tauc's plot, respectively. All films were transparent with a transmittance between 86 and 91 % and all bandgap values were around 3.2 eV.

In terms of structure and morphological characterization, the studies were made on samples of IGZO (1:3:1) with 5 layers. With SEM-FIB it was possible to have a cross-section image of a device, were the IGZO layer had 50 nm of thickness and all layers were clear and distinguished. AFM was performed to study the influence of the annealing temperature on the bottom electrode. By the results, the electrode layer is smooth at the temperatures used to deposit the IGZO active layer. Also, XPS analysis revealed that at the surface the sample annealed at 300 ºC had more M-O-M bonds, whereas the sample annealed at 200 ºC had more presence of M-OH bonds. Depth profile spectra of both samples were obtained, which revealed that near the bottom electrode In, Ga and Zn had more metallic states present.

One big part of this work relied on the electrical characterization, where it was possible to study the memristors behaviors and possible applications. At the beginning the important was to understand, which condition had most of working devices by analyzing the pristine maps and yield. The results demonstrated that an increase in layers was favorable for all conditions. However, IGZO 1:2:1 thin films condition were too conductive. As for IGZO 1:3:1, devices with 1 and 3 layers were also too conductive, but memristors with 5 and 7 layers at both temperatures showed potential to proceed with electrical characterization tests. From those devices, cycling tests revealed good endurance with higher variability on devices annealed at 200 ºC. The devices were capable of retention for 10^5 s with an $R_{ON/OFF}$ of 10^2 s. It was concluded that the best condition for an acceptable memristor was a device with 7 layers annealed at 300 º C, that had MLC feature up to 2^3 bits of storage. Due to the possibility of achieving several resistance states, pulse measurements tests were performed to study the synaptic behavior of the device. The memristor was able to perform potentiation and depression and, pulse interval time was crucial to obtain a gradual response. Also, the STDP was analyzed with a conductance response higher when time between pulses were smaller, demonstrating the PPF effect. Temperature analysis was the last study that revealed the memristor has a semiconductor type behavior, confirming that the V_o are responsible for the conductivity of the device.

Combining material and electrical characterization it can be concluded that the 200 ºC annealing is not sufficient for a good memristor performance, since the incomplete reaction does not form completely the metal oxide. The presence of organic elements interferes with the variability in electrical performance of the devices

processed at lower temperatures. However, the increase in the number of layers attenuated some of these problems.

Finally, this work was a step towards to the future of electronics, it brought together solution-based devices, emergent memories and neuromorphic applications. It was proven that solution-based memristors have electrical properties as good as the vacuum fabricated ones, with less damage to the environment and lower-cost. Also, it brings the possibility of scalability and large manufacturing by using printing techniques.

In spite of the progresses made in this work, there are still questions that remain unanswered and other paths to explore. Based on the results obtained here, some suggestions for future work are:

- Do material characterization, specifically SEM-FIB and XPS, to the samples with 7 IGZO layers, annealed at both temperatures. With these studies, it would be possible to compare the differences in the structure between 5 and 7 layers, understanding better the influence of the increase in layers;
- Improve the fabrication process by reducing annealing time. For each deposited IGZO layer, it is necessary 30 min of annealing and 10 min of UV treatment, resulting in a very time consuming method;
- Increase the number of IGZO layers to obtain a 100 % yield in a sample;
- Fabricate similar memristors by inkjet printing. Using the same IGZO solution to form the ink can be a way to solve the problem of uniformity in the samples;
- Reduce the processing temperature of IGZO memristors by combining thermal annealing with UV irradiation. This will assure their compatibility with low-cost flexible substrates.

5 References

[1] *Advances in Non-Volatile Memory and Storage Technology*. 2019.

[2] E. Fortunato, P. Barquinha, and R. Martins, "Oxide Semiconductor Thin-Film Transistors: A Review of Recent Advances," *Adv. Mater.*, vol. 24, no. 22, pp. 2945–2986, Jun. 2012.

[3] K. Ide, K. Nomura, H. Hosono, and T. Kamiya, "Electronic Defects in Amorphous Oxide Semiconductors: A Review," *Phys. status solidi*, vol. 216, no. 5, p. 1800372, Mar. 2019.

[4] "Transparent Oxide Electronics: From Materials to Devices | Wiley." [Online]. Available: https://www.wiley.com/en-us/Transparent+Oxide+Electronics%3A+From+Materials+to+Devices-p-9780470683736. [Accessed: 04-Mar-2021].

[5] X. Yu, T. J. Marks, and A. Facchetti, "Metal oxides for optoelectronic applications," *Nat. Mater.*, vol. 15, no. 4, pp. 383–396, Mar. 2016.

[6] K. Nomura, H. Ohta, A. Takagi, T. Kamiya, M. Hirano, and H. Hosono, "Room-temperature fabrication of transparent flexible thin-film transistors using amorphous oxide semiconductors," *Nature*, vol. 432, no. 7016, pp. 488–492, Nov. 2004.

[7] M. S. Kim *et al.*, "Effects of the oxygen vacancy concentration in InGaZnO-based resistance random access memory," *Appl. Phys. Lett.*, vol. 101, no. 24, p. 243503, Dec. 2012.

[8] Y. H. Hwang, I. Hwang, and W. J. Cho, "Composition-ratio influence on resistive switching behavior of solution-processed InGaZnO-based thin-film," *J. Nanosci. Nanotechnol.*, vol. 14, no. 11, pp. 8196–8200, Nov. 2014.

[9] W. Hu, L. Zou, X. Chen, N. Qin, S. Li, and D. Bao, "Highly uniform resistive switching properties of amorphous InGaZnO thin films prepared by a low temperature photochemical solution deposition method," *ACS Appl. Mater. Interfaces*, vol. 6, no. 7, pp. 5012–5017, Apr. 2014.

[10] K. Nomura, H. Ohta, A. Takagi, T. Kamiya, M. Hirano, and H. Hosono, "Room-temperature fabrication of transparent flexible thin-film transistors using amorphous oxide semiconductors," *Nature*, vol. 432, no. 7016, pp. 488–492, Nov. 2004.

[11] T. Iwasaki *et al.*, "Combinatorial approach to thin-film transistors using multicomponent semiconductor channels: An application to amorphous oxide semiconductors in In-Ga-Zn-O system," *Appl. Phys. Lett.*, vol. 90, no. 24, p. 242114, Jun. 2007.

[12] H. Hosono, "Ionic amorphous oxide semiconductors: Material design, carrier transport, and device application," *J. Non. Cryst. Solids*, vol. 352, no. 9-20 SPEC. ISS., pp. 851–858, Jun. 2006.

[13] P. K. Nayak, M. N. Hedhili, D. Cha, and H. N. Alshareef, "High performance solution-deposited amorphous indium gallium zinc oxide thin film transistors by oxygen plasma treatment," *Appl. Phys. Lett.*, vol. 100, no. 20, p. 202106, May 2012.

[14] Moreira *et al.*, "Tailoring IGZO Composition for Enhanced Fully Solution-Based Thin Film Transistors," *Nanomaterials*, vol. 9, no. 9, p. 1273, Sep. 2019.

[15] M. J. Rozenberg, M. J. Sánchez, R. Weht, C. Acha, F. Gomez-Marlasca, and P. Levy, "Mechanism for bipolar resistive switching in transition-metal oxides," *Phys. Rev. B - Condens. Matter Mater. Phys.*, vol. 81, no. 11, p. 115101, Mar. 2010.

[16] J. Rosa *et al.*, "Memristors Using Solution-Based IGZO Nanoparticles," *ACS Omega*, vol. 2, no. 11, pp. 8366–8372, Nov. 2017.

[17] L. Li *et al.*, "Resistive switching IGZO micro-arrays realized through UV assisted photochemical solution method," *J. Sol-Gel Sci. Technol.*, vol. 88, no. 3, pp. 601–608, Dec. 2018.

[18] D. Lee, M. C. Chun, H. Ko, B. S. Kang, and J. Kim, "Highly stable, solution-processed quaternary oxide thin film-based resistive switching random access memory devices via global and local stoichiometric manipulation strategy," *Nanotechnology*, vol. 31, no. 24, p. 245202, Mar. 2020.

[19] S. Song *et al.*, "Solution-processed oxide semiconductor-based artificial optoelectronic synapse array for spatiotemporal synaptic integration," *J. Alloys Compd.*, vol. 857, p. 158027, Mar. 2021.

[20] S. Y. Min and W. J. Cho, "High-performance resistive switching in solution-derived igzo:N memristors by microwave-assisted nitridation," *Nanomaterials*, vol. 11, no. 5, p. 1081, Apr. 2021.

[21] K. K. H. Smithe, S. V. Suryavanshi, M. Muñoz Rojo, A. D. Tedjarati, and E. Pop, "Low Variability in Synthetic Monolayer MoS2 Devices," *ACS Nano*, vol. 11, no. 8, pp. 8456–8463, Aug. 2017.

[22] G. S. Tang *et al.*, "Resistive switching with self-rectifying behavior in Cu/SiOx/Si structure fabricated by plasma-oxidation," *J. Appl. Phys.*, vol. 113, no. 24, p. 244502, Jun. 2013.

[23] A. Chen, S. Haddad, Y. C. Wu, T. N. Fang, S. Kaza, and Z. Lan, "Erasing characteristics of Cu2 O metal-insulator-metal resistive switching memory," *Appl. Phys. Lett.*, vol. 92, no. 1, p. 013503, Jan. 2008.

[24] Z. Yan, Y. Guo, G. Zhang, and J.-M. Liu, "High-Performance Programmable Memory Devices Based on Co-Doped BaTiO3," *Adv. Mater.*, vol. 23, no. 11, pp. 1351–1355, Mar. 2011.

[25] C. Chen, C. Song, J. Yang, F. Zeng, and F. Pan, "Oxygen migration induced resistive switching effect and its thermal stability in W/TaO x/Pt structure," *Appl. Phys. Lett.*, vol. 100, no. 25, p. 253509, Jun. 2012.

[26] G. Chen, C. Song, and F. Pan, "Improved resistive switching stability of Pt/ZnO/CoO x /ZnO/Pt structure for nonvolatile memory devices," *Rare Met.*, vol. 32, no. 6, pp. 544–549, Dec. 2013.

[27] N. Casa Branca *et al.*, "2D Resistive Switching Based on Amorphous Zinc–Tin Oxide Schottky Diodes," *Adv. Electron. Mater.*, vol. 6, no. 2, p. 1900958, Feb. 2020.

[28] J. Deuermeier, A. Kiazadeh, A. Klein, R. Martins, and E. Fortunato, "Multi-Level Cell Properties of a Bilayer Cu2O/Al2O3 Resistive Switching Device," *Nanomaterials*, vol. 9, no. 2, p. 289, Feb. 2019.

[29] Y. S. Rim, H. S. Lim, and H. J. Kim, "Low-temperature metal-oxide thin-film transistors formed by directly photopatternable and combustible solution synthesis," *ACS Appl. Mater. Interfaces*, vol. 5, no. 9, pp. 3565–3571, May 2013.

[30] S. J. Kim, G. H. Kim, D. L. Kim, D. N. Kim, and H. J. Kim, "InGaZnO thin-film transistors with YHfZnO gate insulator by solution process," *Phys. status solidi*, vol. 207, no. 7, pp. 1668–1671, May 2010.

[31] N. Gergel-Hackett *et al.*, "A Flexible Solution-Processed Memristor," 2009.

[32] E. Carlos *et al.*, "Boosting Electrical Performance of High-κ Nanomultilayer Dielectrics and Electronic Devices by Combining Solution Combustion Synthesis and UV Irradiation," *ACS Appl. Mater. Interfaces*, vol. 9, no. 46, pp. 40428–40437, Nov. 2017.

[33] E. Carlos, A. Kiazadeh, J. Deuermeier, R. Branquinho, R. Martins, and E. Fortunato, "Critical role of a double-layer configuration in solution-based unipolar resistive switching memories," *Nanotechnology*, vol. 29, no. 34, p. 345206, Jun. 2018.

[34] R. Branquinho *et al.*, "Towards environmental friendly solution-based ZTO/AlOx TFTs," *Semicond.*

Sci. Technol., vol. 30, no. 2, p. 24007, 2015.

[35] K. H. Jang, S. M. Oh, H. M. An, and W. J. Cho, “Solution-processed high-k thin films as a resistive switching for ReRAM applications,” *Curr. Appl. Phys.*, vol. 14, no. 3, pp. 462–466, Mar. 2014.

[36] E. Carlos, R. Branquinho, R. Martins, A. Kiazadeh, and E. Fortunato, “Recent Progress in Solution-Based Metal Oxide Resistive Switching Devices,” *Adv. Mater.*, vol. 2004328, pp. 1–37, 2020.

[37] B. Sharma and M. K. Rabinal, “A simple dip coat patterning of aluminum oxide to constitute a bistable memristor,” *Mater. Res. Express*, vol. 3, no. 12, p. 126302, Dec. 2016.

[38] B. Huber, P. B. Popp, M. Kaiser, A. Ruediger, and C. Schindler, “Fully inkjet printed flexible resistive memory,” *Appl. Phys. Lett.*, vol. 110, no. 14, p. 143503, Apr. 2017.

[39] J. W. Park, B. H. Kang, and H. J. Kim, “A Review of Low-Temperature Solution-Processed Metal Oxide Thin-Film Transistors for Flexible Electronics,” *Adv. Funct. Mater.*, vol. 30, no. 20, p. 1904632, May 2020.

[40] H. C. You and G. K. Lin, “Solution-processed ZnO thin films for low voltage and low temperature application in flexible resistive random access memory,” *Thin Solid Films*, vol. 616, pp. 728–732, Oct. 2016.

[41] Y. Pan *et al.*, “Mimicking synaptic plasticity and learning behaviours in solution processed SnO2 memristor,” *J. Alloys Compd.*, vol. 757, pp. 496–503, Aug. 2018.

[42] J. Jang and V. Subramanian, “Effect of electrode material on resistive switching memory behavior of solution-processed resistive switches: Realization of robust multi-level cells,” *Thin Solid Films*, vol. 625, pp. 87–92, Mar. 2017.

[43] S. Park, C. H. Kim, W. J. Lee, S. Sung, and M. H. Yoon, “Sol-gel metal oxide dielectrics for all-solution-processed electronics,” *Materials Science and Engineering R: Reports*, vol. 114. Elsevier Ltd, pp. 1–22, 01-Apr-2017.

[44] “Sol-Gel Science: The Physics and Chemistry of Sol-Gel Processing - C. Jeffrey Brinker, George W. Scherer - Google Livros.” [Online]. Available: https://books.google.pt/books?hl=pt-PT&lr=&id=CND1BAAAQBAJ&oi=fnd&pg=PP1&dq=C.+J.+Brinker,+G.+W.+Scherer,+Sol-Gel+Science:+The+Physics+and+Chemistry+of+Sol-Gel+Processing,+Academic+Press,+San+Diego,+CA+1990&ots=aftMG7UdeC&sig=aXvSry2Tequy9IhBWiKY9q20zFY&redir_esc=y#v=onepage&q&f=false. [Accessed: 10-Mar-2021].

[45] E. Carlos, S. Dellis, N. Kalfagiannis, L. Koutsokeras, D. C. Koutsogeorgis, R. Branquinho, R. Martins and E. Fortunato, “Laser induced ultrafast combustion synthesis of solution-based AlO: Xfor thin film transistors,” *J. Mater. Chem. C*, vol. 8, no. 18, pp. 6176–6184, May 2020.

[46] E. Carlos, R. Branquinho, A. Kiazadeh, P. Barquinha, R. Martins, and E. Fortunato, “UV-Mediated Photochemical Treatment for Low-Temperature Oxide-Based Thin-Film Transistors,” *ACS Appl. Mater. Interfaces*, vol. 8, no. 45, pp. 31100–31108, Nov. 2016.

[47] E. Carlos, R. Martins, E. Fortunato, and R. Branquinho, “Solution Combustion Synthesis: Towards a Sustainable Approach for Metal Oxides,” *Chem. - A Eur. J.*, vol. 26, no. 42, pp. 9099–9125, 2020.

[48] T. W. Hickmott, “Low-frequency negative resistance in thin anodic oxide films,” *J. Appl. Phys.*, 1962.

[49] J. G. Simmons and R. R. Verderberf, “New conduction and reversible memory phenomena in thin insulating films,” *Proc. R. Soc. London. Ser. A. Math. Phys. Sci.*, vol. 301, no. 1464, pp. 77–102, Oct. 1967.

[50] S. Q. Liu, N. J. Wu, and A. Ignatiev, “Electric-pulse-induced reversible resistance change effect in

magnetoresistive films," *Appl. Phys. Lett.*, vol. 76, no. 19, pp. 2749–2751, May 2000.

[51] D. B. Strukov, G. S. Snider, D. R. Stewart, and R. S. Williams, "The missing memristor found," *Nature*, 2008.

[52] F. Hui, E. Grustan-Gutierrez, S. Long, Q. Liu, A. K. Ott, A. C. Ferrari and M. Lanza, "Graphene and Related Materials for Resistive Random Access Memories," *Adv. Electron. Mater.*, vol. 3, no. 8, p. 1600195, Aug. 2017.

[53] M. Sako, Y. Watanabe, T. Nakajima, J. Sato, K. Muraoka, M. Fujiu, F. Kono, M. Nakagawa, M. Masuda, K. Kato, Y. Terada, Y. Shimizu and X. Wang., "A low power 64 Gb MLC NAND-flash memory in 15 nm CMOS technology," *IEEE J. Solid-State Circuits*, vol. 51, no. 1, pp. 196–203, Jan. 2016.

[54] Y. Kim, II H. Park, S. Cho, J. Yun, J. H. Lee, D. Kim, S. Lee, S. Park, D. Lee, W. B. Sim, W. Kim and H. Shin, "A vertical 4-bit SONOS flash memory and a unique 3-D vertical nor array structure," *IEEE Trans. Nanotechnol.*, vol. 9, no. 1, pp. 70–77, Jan. 2010.

[55] S. H. Jo, T. Chang, I. Ebong, B. B. Bhadviya, P. Mazumder, and W. Lu, "Nanoscale memristor device as synapse in neuromorphic systems," *Nano Lett.*, vol. 10, no. 4, pp. 1297–1301, Apr. 2010.

[56] B. Govoreanu, G. S. Kar, Y-Y. Chen, V. Paraschiv, S. Kubicek, A. Fantini, I. P. Radu, L. Goux, S. Clima, R. Degraeve, N. Jossart, O. Richard, T. Vandeweyer, K, Seo and P. Hendrickx, "10×10nm 2 Hf/HfO x crossbar resistive RAM with excellent performance, reliability and low-energy operation," in *Technical Digest - International Electron Devices Meeting, IEDM*, 2011.

[57] M. K. Gupta and M. Hasan, "Robust High Speed Ternary Magnetic Content Addressable Memory," *IEEE Trans. Electron Devices*, vol. 62, no. 4, pp. 1163–1169, Apr. 2015.

[58] A. D. Kent and D. C. Worledge, "A new spin on magnetic memories," *Nature Nanotechnology*, vol. 10, no. 3. Nature Publishing Group, pp. 187–191, 05-Mar-2015.

[59] G. W. Burr, M. J. Brightsky, A. Sebastian, H-Y. Wu, S. Kim, N. E. Sosa, N. Papandreou, H-L. Lung and H. Pozidis, "Recent Progress in Phase-Change Memory Technology," *IEEE J. Emerg. Sel. Top. Circuits Syst.*, vol. 6, no. 2, pp. 146–162, Jun. 2016.

[60] R. Waser, R. Dittmann, G. Staikov, and K. Szot, "Redox-Based Resistive Switching Memories - Nanoionic Mechanisms, Prospects, C. R. Waser, R. Dittmann, G. Staikov, and K. Szot, 'Redox-Based Resistive Switching Memories - Nanoionic Mechanisms, Prospects, and Challenges,' Adv. Mater., vol. 21, no. ," *Adv. Mater.*, vol. 21, no. 25–26, pp. 2632–2663, Jul. 2009.

[61] I. Valov, "Redox-Based Resistive Switching Memories (ReRAMs): Electrochemical Systems at the Atomic Scale," *ChemElectroChem*, vol. 1, no. 1, pp. 26–36, Jan. 2014.

[62] L. Goux and I. Valov, "Electrochemical processes and device improvement in conductive bridge RAM cells," *Phys. status solidi*, vol. 213, no. 2, pp. 274–288, Feb. 2016.

[63] D. Ielmini, R. Bruchhaus, and R. Waser, "Thermochemical resistive switching: materials, mechanisms, and scaling projections," *Phase Transitions*, vol. 84, no. 7, pp. 570–602, Jul. 2011.

[64] M. Lübben, P. Karakolis, V. Ioannou-Sougleridis, P. Normand, P. Dimitrakis, and I. Valov, "Graphene-Modified Interface Controls Transition from VCM to ECM Switching Modes in Ta/TaO $_x$ Based Memristive Devices," *Adv. Mater.*, vol. 27, no. 40, pp. 6202–6207, Oct. 2015.

[65] A. Kindsmüller, A. Meledin, J. Mayer, R. Waser, and D. J. Wouters, "On the role of the metal oxide/reactive electrode interface during the forming procedure of valence change ReRAM devices," *Nanoscale*, vol. 11, no. 39, pp. 18201–18208, Oct. 2019.

[66] M. Pereira, J. Deuermeier, R. Nogueira, P. A. Carvalho, R. Martins, E. Fortunato and A. Kiazadeh ,"Noble-Metal-Free Memristive Devices Based on IGZO for Neuromorphic Applications," *Adv. Electron. Mater.*, vol. 6, no. 10, p. 2000242, Oct. 2020.

[67] S. Kim, H. Kim, S. Hwang, M.-H. Kim, Y.-F. Chang, and B.-G. Park, "Analog Synaptic Behavior of a Silicon Nitride Memristor," *ACS Appl. Mater. Interfaces*, vol. 9, no. 46, pp. 40420–40427, Nov. 2017.

[68] Y. Park and J.-S. Lee, "Artificial Synapses with Short- and Long-Term Memory for Spiking Neural Networks Based on Renewable Materials," *ACS Nano*, vol. 11, no. 9, pp. 8962–8969, Sep. 2017.

[69] X. Hong, D. J. Loy, P. A. Dananjaya, F. Tan, C. Ng, and W. Lew, "Oxide-based RRAM materials for neuromorphic computing," *J. Mater. Sci. 2018 5312*, vol. 53, no. 12, pp. 8720–8746, Feb. 2018.

[70] K. Lu, X. Li, Q. Sun, X. Pang, J. Chen, T. Minari, X. Liu and Y. Song, "Solution-processed electronics for artificial synapses," *Mater. Horizons*, vol. 8, no. 2, pp. 447–470, Feb. 2021.

[71] M. Xie, S. Wu, Z. Chen, Q. Khan, X. Wu, S. Shao and Z. Cui, "Performance improvement for printed indium gallium zinc oxide thin-film transistors with a preheating process," *RSC Adv.*, vol. 6, no. 47, pp. 41439–41446, Apr. 2016.

[72] D. Salgueiro, A. Kiazadeh, R. Branquinho, L. Santos, P. Barquinha, R. Martins and E. Fortunato, "Solution based zinc tin oxide TFTs: the dual role of the organic solvent," *J. Phys. D. Appl. Phys.*, vol. 50, no. 6, p. 065106, Jan. 2017.

[73] P. Barquinha, *"Transparent Oxide Thin-Film Transistor: production, characterization and integration"*, FCT-UNL, 2010.

[74] K. Moon, S. Lim, J. Park, C. Sung, S. Oh, J. Woo, J. Lee and H. Hwang, "RRAM-based synapse devices for neuromorphic systems," *Faraday Discuss.*, vol. 213, no. 0, pp. 421–451, Feb. 2019.

[75] Y. Huang, Z. Shen, Y. Wu, X. Wang, S. Zhang, X. Shi and H. Zeng, "Amorphous ZnO based resistive random access memory," *RSC Adv.*, vol. 6, no. 22, pp. 17867–17872, Feb. 2016.

Annexes

Annex A – IGZO Redox Reactions

The synthesis of IGZO by SCS involves reactions of reduction of metallic nitrates and oxidation of the fuel used [47], as presented in Table A.1.

Table A.1 - Reduction and oxidation reactions.

	Reduction Reaction
Indium nitrate hydrate	$2In(NO_3)_3{\cdot}H_2O \rightarrow In_2O_3 + 2H_2O + 3N_2 + \frac{15}{2}O_2$
Gallium nitrate hydrate	$2Ga(NO_3)_3{\cdot}H_2O \rightarrow Ga_2O_3 + 2H_2O + 3N_2 + \frac{15}{2}O_2$
Zinc nitrate hexahydrate	$Zn(NO_3)_2{\cdot}6H_2O \rightarrow ZnO + 6H_2O + N_2 + \frac{5}{2}O_2$
	Oxidation Reaction
Urea	$CO(NH_2)_2 + \frac{3}{2}O_2 \rightarrow 2H_2O + CO_2 + N_2$
2 – Methoxyethanol	$C_3H_8O_2 + 4O_2 \rightarrow 4H_2O + 3CO_2$

The complete combustion reaction is the combination of reduction and oxidation reactions, as shown in Table A.2. There is formation of gaseous products, including H_2O, N_2, CO_2 and O_2 that are released. In this work, urea is used as fuel.

Table A.2 - Overall reaction given by the combination of reduction and oxidation reaction.

Precursor	**Fuel**	**Overall reaction**
Indium nitrate hydrate	Urea	$2In(NO_3)_3{\cdot}H_2O + CO(NH_2)_2 \rightarrow In_2O_3 + 4H_2O + 4N_2 + CO_2 + 6O_2$
Gallium nitrate hydrate		$2Ga(NO_3)_3{\cdot}H_2O + CO(NH_2)_2 \rightarrow Ga_2O_3 + 4H_2O + 4N_2 + CO_2 + 6O_2$
Zinc nitrate hexahydrate		$Zn(NO_3)_2{\cdot}6H_2O + CO(NH_2)_2 \rightarrow ZnO + 8H_2O + 2N_2 + CO_2 + O_2$

To determine the correct stoichiometry proportion of oxidizer and fuel needed, it is used the Jain method. This method relates the amount of reagents and their reducing and oxidizing valences, the right molar ratio of the reactants is ensured. The relation is given by Equation 2 [47]:

$$\varphi = \frac{RV}{OV} n \quad (2)$$

Where φ is the fuel/oxidizer ratio, RV and OV are reducing valence and oxidizing valence, respectively, and n is the number of moles per mole of oxidant. For the right stoichiometry ratio with balanced species, Jain's methos has to be calculated with $\varphi = 1$. Indium, gallium, zinc, carbon and hydrogen are considered reducing agents with corresponding valences of +3, +3, +2, +4 and +1, respectively. Whereas oxygen and nitrogen have corresponding valences of -2 and 0, respectively, being considered oxidizer agents [47]. In this case, the calculations of the oxidizer and reducing reagents are presented in Table A.3.

Table A.3 - Valence of all reagents.

Reagent	**Chemical Formula**	**Calculation**	**Total**
Oxidizer reagent (OV)	$In(NO_3)_3$	$3 + (3 \times 0) + [3 \times 3 \times (-2)]$	-15
	$Ga(NO_3)_3$	$3 + (3 \times 0) + [3 \times 3 \times (-2)]$	-15
	$Zn(NO_3)_2$	$2 + (2 \times 0) + [2 \times 3 \times (-2)]$	-10
Reducing reagent (RV)	$CO(NH_2)_2$	$4 + (-2) + (2 \times 0) + (2 \times 2 \times 1)$	+6

Thus, with the calculations of the valence of the reagents, the number of moles needed to ensure the stoichiometry of the redox reaction can be determined, as depicted in Table A.4.

Table A.4 - Number of moles (n) to ensure the stoichiometry of the redox reaction.

Precursor	**Fuel**	**φ**	***n***
Indium nitrate hydrate	Urea	1	5/2
Gallium nitrate hydrate			5/2
Zinc nitrate hexahydrate			5/3

Lastly, the complete reactions with the right number of moles to ensure the stoichiometry of the redox reaction are described in Table A.5.

Table A.5 - Overall reactions with the correct stoichiometry.

Precursor	**Fuel**	**Overall reaction**
Indium nitrate hydrate	Urea	$2In(NO_3)_3 \cdot 2H_2O + 5CO(NH_2)_2 \rightarrow In_2O_3 + 14H_2O + 8N_2 + 5CO_2$
Gallium nitrate hydrate		$2Ga(NO_3)_3 \cdot 2H_2O + 5CO(NH_2)_2 \rightarrow Ga_2O_3 + 14H_2O + 8N_2 + 5CO_2$
Zinc nitrate hexahydrate		$3Zn(NO_3)_2 \cdot 6H_2O + 5CO(NH_2)_2 \rightarrow 3ZnO + 28H_2O + 8N_2 + 5CO_2$

Annex B – Calculation of E_{opt} of IGZO Thin Films

Through the absorption coefficient (α) it is possible to determine the E_{opt} of the IGZO thin films by using Equation 3:

$$\alpha = \frac{1}{d}\ln\left(\frac{1}{1-A}\right) \quad (3)$$

where d is the thickness and A is the optical absorption of the thin film. Since A corresponds to 1-T-R, where R is reflectance and can be neglected, the approximate values of α can be calculated. The E_{opt} was determined by Tauc's relation as described in Equation 4,

$$\alpha^{x} \propto h\nu - E_{opt} \quad (4)$$

Where h is the Planck constant, ν is the photon frequency and x is a value related to the transition type. In case of amorphous semiconductors, the x can be considered 0.5 as non-direct optical transitions are allowed [73]. In Figure B.1 is represented the Tauc plots used to calculate E_{opt} of each IGZO condition studied and Table B.1 depicts the coefficient of determination (R^2) of each linear fit made.

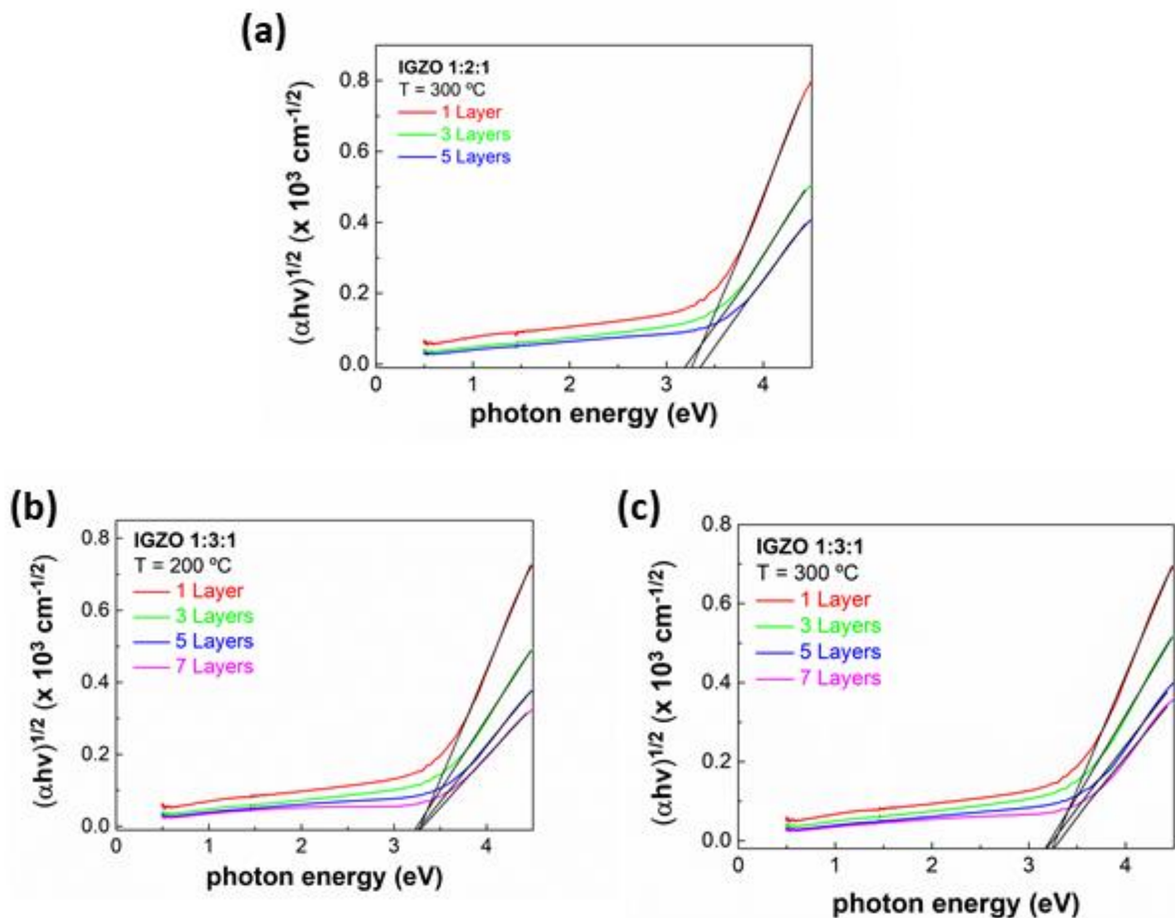

Figure B.1 - Tauc-bandgap plots to calculate E_{opt} of each condition studied.

Table B.1 - R^2 of each linear fit in Tauc plots.

Number of Layers	**200 ºC**	**300 ºC**	
	1:3:1	**1:3:1**	**1:2:1**
1	0.9982	0.9972	0.9978
3	0.9974	0.9956	0.9991
5	0.9980	0.9904	0.9992
7	0.9991	0.9912	———

Annex C – XPS depth profile spectra'

XPS depth profile spectra' of Ga 2p 3/2, Zn 2p 3/2, In 3d 5/2 and Pt 4f of samples with 5 IGZO (1:3:1) layers annealed at 200 and 300 ºC are depicted in Figure C.1 and Figure C.2, respectively.

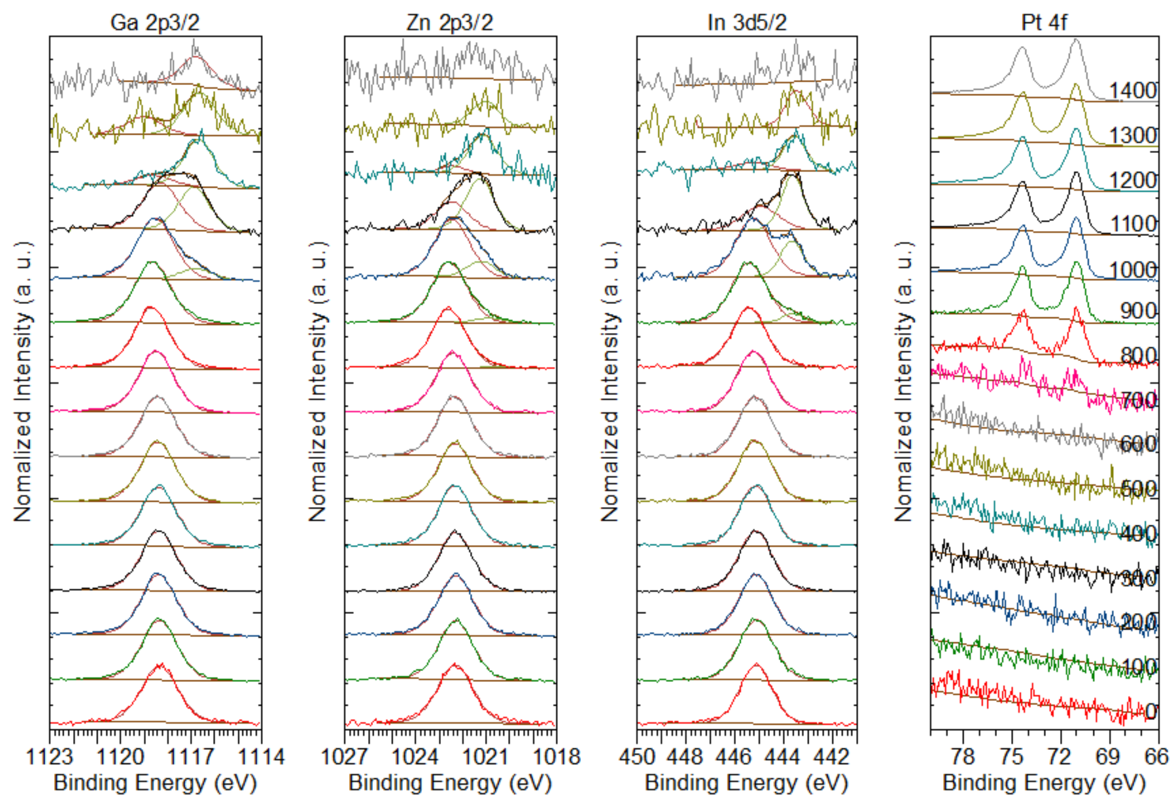

Figure C.1 - XPS depth profile spectra after each etching of Ga $2p_{3/2}$, Zn $2p_{3/2}$, In $5d_{3/2}$ and Pt 4f of a 5 layered device annealed at 200 ºC.

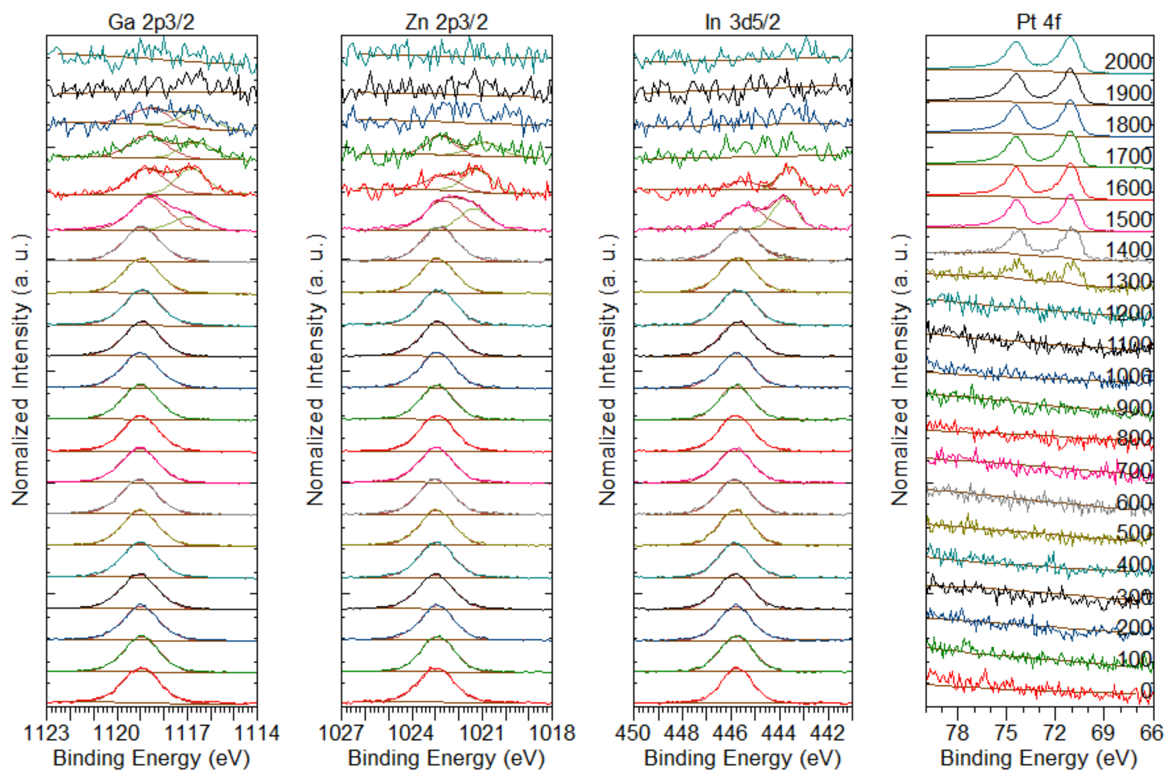

Figure C.2 – XPS depth profile spectra after each etching of Ga $2p_{3/2}$, Zn $2p_{3/2}$, In $5d_{3/2}$ and Pt 4f of a 5 layered device annealed at 300 ºC

Annex D – Pristine Maps

Figure D.2, Figure D.3, Figure D.4 and Figure D.5 show the pristine maps of all samples studied. The voltage sweep was from -0.5 to 0.5 V and the CC was 1 mA or 10 mA. Pristine curves presented in green are considered working devices, while red pristine curves are non-working devices. Figure D.1 represents a schematic of a sample with Kapton tape.

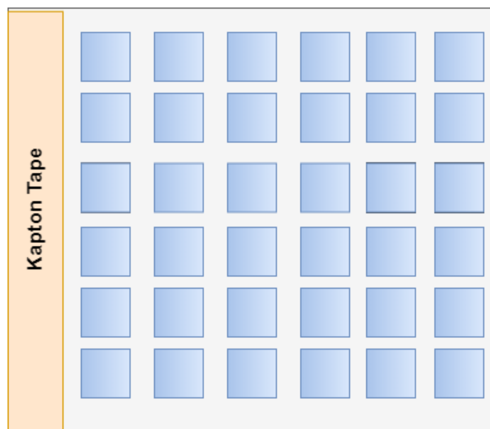

Figure D.1 - Representation of a produced sample with Kapton tape.

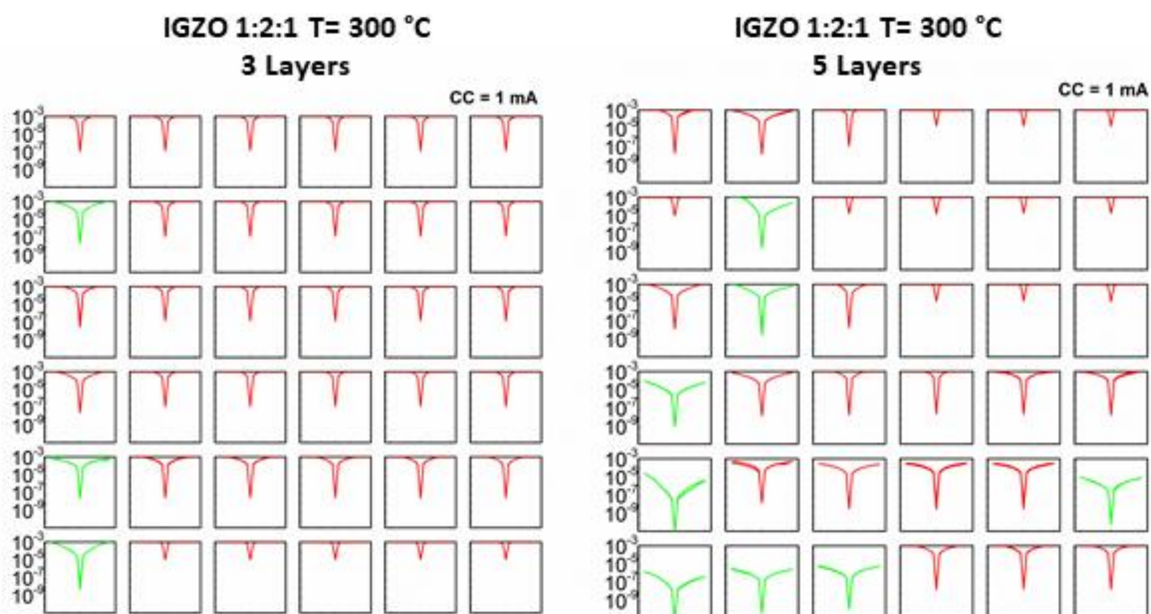

Figure D.2 - Pristine maps of samples: IGZO molar proportion of 1:2:1 and annealed at 300 ºC, with 3 (left) and 5 layers (right).

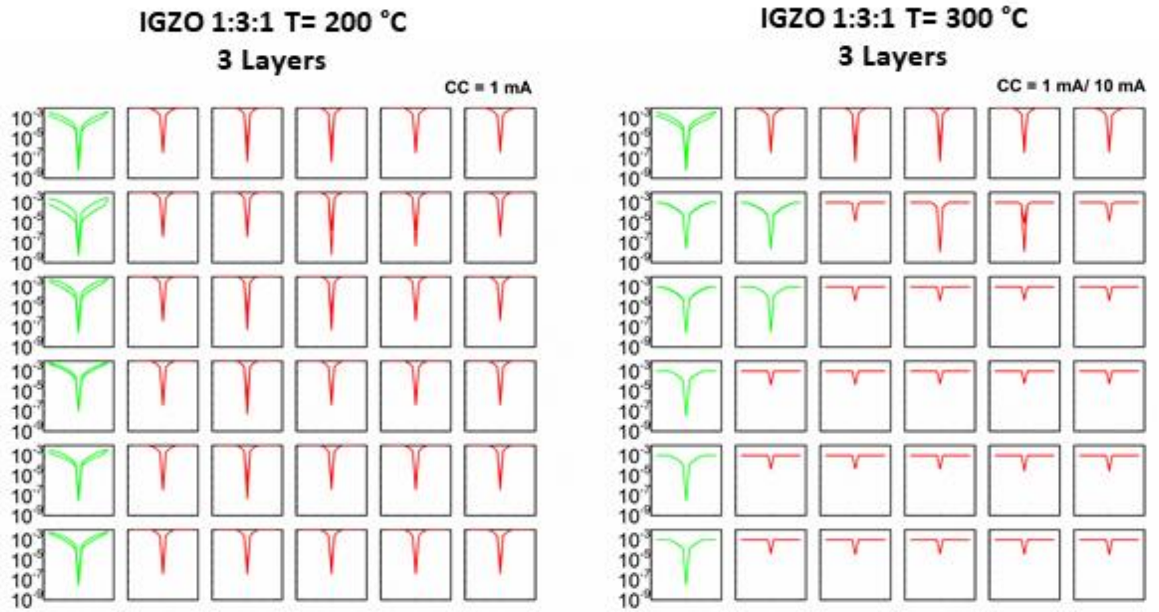

Figure D.3 - Pristine maps of IGZO 1:3:1 samples with 3 layers annealed at 200 ºC (left) and 300 ºC (right).

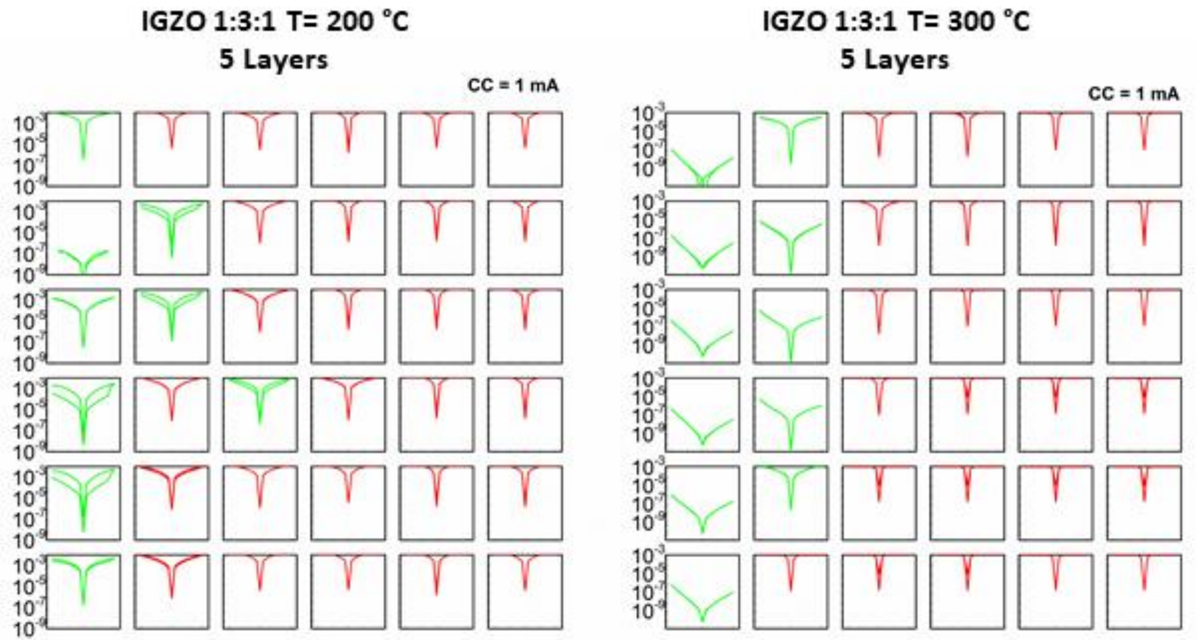

Figure D.4 - Pristine maps of IGZO 1:3:1 samples with 5 layers annealed at 200 ºC (left) and 300 ºC (right).

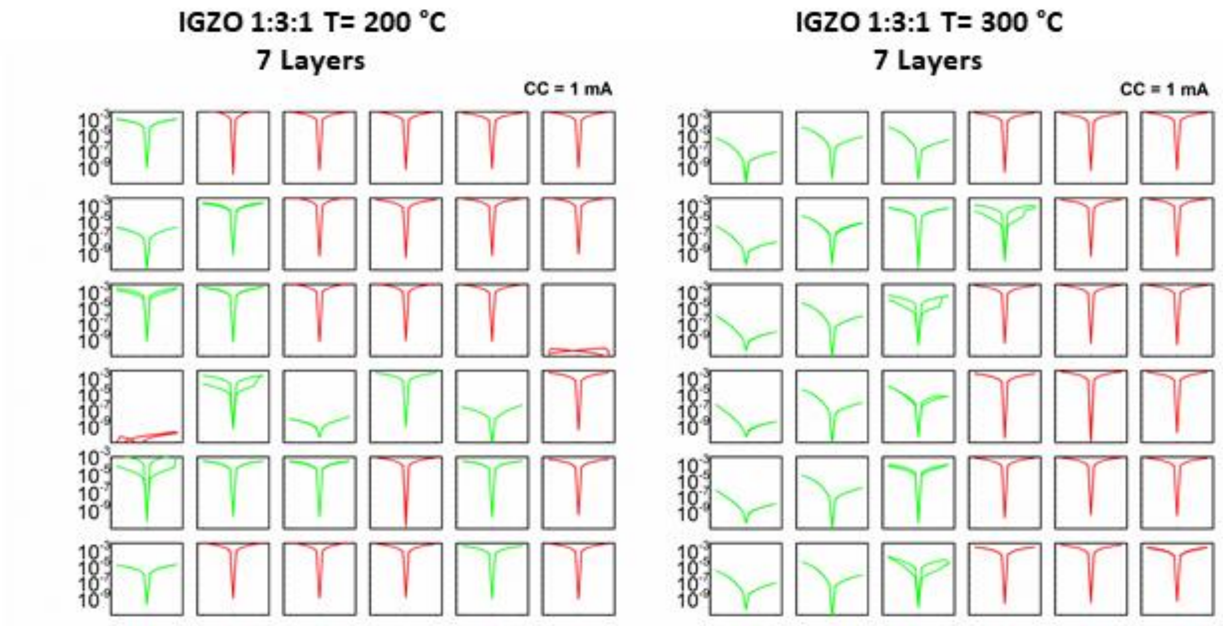

Figure D.5 - Pristine maps of IGZO 1:3:1 samples with 7 layers annealed at 200 ºC (left) and 300 ºC (right).

2021

RAQUEL AZEVEDO MARTINS

SOLUTION-BASED METAL OXIDE SEMICONDUCTOR MEMRISTOR

NOVA

NOVA SCHOOL OF SCIENCE & TECHNOLOGY